The Astrophysical Journal Supplement Series, 147:145–166, 2003 July

AN ARCHIVE OF *IUE* LOW-DISPERSION SPECTRA OF THE WHITE DWARF STARS

J. B. Holberg
Lunar and Planetary Laboratory, University of Arizona; holberg@argus.lpl.arizona.edu

M. A. Barstow
Department of Physics and Astronomy, University of Leicester, University Road, Leicester, LE 1 7RH, UK; mab@star.le.ac.uk

and

M. R. Burleigh
Department of Physics and Astronomy, University of Leicester, University Road, Leicester, LE 1 7RH, UK; mbu@star.le.ac.uk
Received 2002 November 4; accepted 2003 February 19

ABSTRACT

We have produced an archive of the ultraviolet low-dispersion spectra for the full set of white dwarf stars observed with the *International Ultraviolet Explorer* (*IUE*) satellite over the course of its 18 yr mission. This archive contains the spectra of 322 individual degenerate stars which have been processed to optimize the signal-to-noise for each star. In particular, all spectra have been corrected for residual temporal and thermal effects and placed on the *Hubble Space Telescope* Faint Object Spectrograph absolute flux scale using procedures described by Massa & Fitzpatrick. Wherever possible, multiple observations of individual stars have been co-added to further enhance signal-to-noise and have been combined into a single spectrum including the full 1150 to 3150 Å wavelength region observed by *IUE*. The contents of this spectral archive are described and the details of data reduction procedures are provided, along with the url for access to the electronic files of the processed spectra.

Subject headings: atlases — ultraviolet: stars — white dwarfs

1. INTRODUCTION

The *International Ultraviolet Explorer* (*IUE*) satellite (Kondo et al. 1989 and Boggess et al. 1978a, 1978b) operated successfully from early 1978 until it was turned off in late 1996. During this period, *IUE* was used continually by large segments of the international astronomical community to obtain more than 100,000 ultraviolet spectra of a wide variety of astrophysical targets. One major class of objects observed with *IUE* were the white dwarf stars. In all, more than 300 degenerate stars were observed. These observations led to a number of key discoveries regarding the nature of degenerate stars and their photospheres. We review some of these discoveries in § 4 of this paper. The url for electronic access to the processed spectra is provided in the acknowledgements.

IUE operated in both a low-dispersion spectral mode with a resolution of ~6 Å and a high-dispersion echelle mode with a resolution of ~0.2 Å. About 89% of the white dwarf spectra were obtained in the low-dispersion mode. Although numerous authors have published results based on individual observations, as well as specialized studies of classes of degenerate stars, a unified archive of all low-dispersion white dwarf spectra has not been available. Now that the *IUE* mission is complete, the need for such an archive is warranted on several grounds. First, *IUE* data processing procedures matured dramatically over the course of the mission, so that the quality of an extracted spectrum produced today greatly exceeds that possible during the early part of the mission. This is particularly true now that the entire *IUE* data set has been reprocessed by NASA using the NEWSIPS (New Spectroscopic Image Procession System) data reduction procedures (Nichols & Linsky 1996, hereafter NL96). NEWSIPS incorporates many available data processing improvements that have resulted in more uniformity among spectra and better signal-to-noise (S/N) than the previous IUESIPS data system. Second, complete sets of spectra for all stars are now available. These spectra can be compared and combined to yield even further improvements in quality. By coherently co-adding spectra on a uniform wavelength scale, it is possible to significantly enhance spectral S/N for many stars.

Over its lifetime *IUE* observed some 323 individual degenerate stars of all varieties. The total number of separate exposures represented by these observations exceed 1658. There have been several previous efforts to summarize various aspects and portions of this data set. Wegner & Swanson (1991) published a catalog of low-dispersion spectra for 182 white dwarfs. Bica, Bonatto, & Giovannini (1996) published a library of template spectra representing various spectral types and temperature classes of white dwarfs, which they formed from the *IUE* low-dispersion spectra of 83 white dwarfs. Finally, Holberg, Barstow, & Sion (1998, hereafter HBS) produced an archive of 209 co-added NEWSIPS spectra for 55 degenerate stars observed by *IUE* in echelle mode. In this paper we describe the corresponding companion to the HBS echelle archive: a complete archive of the white dwarfs observed by *IUE* in low dispersion.

In the remainder of this section we briefly describe some general aspects of the *IUE* spectrometers and discuss the salient features of the NEWSIPS data reduction system. This is followed by a brief description of the post-NEWSIPS corrections to the spectra developed by Massa & Fitzpatrick (2000). In our experience, these corrections, greatly enhance the consistency, fidelity, and S/N of NEWSIPS spectra. In § 2 we briefly review the nature and characteristics of *IUE* low-dispersion spectra and describe the procedures used here to reduce, correct, and co-add the spectra. Helpful descriptions of the different formats for the data products

and their availability are presented. In § 3 we summarize the content of the archive data set, illustrate the improvement in spectral S/N, and describe the nature of the final spectra. In § 4 we briefly discuss representative spectra of the different classes of white dwarfs observed with *IUE*.

1.1. *IUE Observations and Spectra*

IUE employed two pairs of redundant UV sensitive videcon cameras. For short wavelengths, from 1150 to 1970 Å, these were designated the short wavelength prime (SWP) and short wavelength redundant (SWR) cameras; however, the latter was seldom used for scientific observations. For long wavelengths, from 1850 to 3200 Å, the long wavelength prime (LWP) and the long wavelength redundant (LWR) cameras were used. The LWR camera was operated almost exclusively until 1983, when it was decommissioned and the LWP became the operative long wavelength detector. *IUE* spectra could be obtained at two resolutions, a high-dispersion echelle mode with $\lambda/\Delta\lambda \sim 10,000$ and a low-dispersion mode with $\lambda/\Delta\lambda \sim 200$. (A full description and summary of *IUE* echelle mode observations of the white dwarf stars is presented in HBS and will not be discussed further here.) Only one camera and spectral mode could be employed at a given time, since the image from each camera had to be read out in real time before the next exposure could begin. Each camera had two focal plane science apertures; a large (10″ x 20″) aperture (LAP) with a rectangular oval shape and a circular small aperture (SAP), 3″ in diameter. Stellar or point source targets could be placed at various locations within the LAP, and exposures were possible in three basic modes: (1) a "trailed" exposure in which the target was slewed along the long dimension the cross dispersion direction, of the LAP, (2) multiple exposures of the target at two or three discrete locations within the LAP, and (3) a single exposure of the target at one location in the LAP. The 3″ SAP was not much larger than the image size, this resulted in 50% or less of the light being transmitted. For white dwarfs, the chief advantage of the SAP was that it transmitted only about 5% of the diffuse geocoronal Lyα background. Observations in the SAP were therefore extremely useful for producing relatively uncontaminated spectra of the intrinsic stellar Lyα profiles, free of the geocoronal line. It was also possible to obtain the spectrum of a star in both large and small apertures, in the same image, by moving the star from one aperture to the other during the course of an exposure, prior to reading out the image.

The *IUE* videcon cameras were nonlinear analog detectors and were subject to a number of geometric, thermal, and temporal effects. The production of calibrated, scientifically useful, spectra from raw images required a number of steps and involved an extensive library of calibration data. Basically, two-dimensional images of the exposed videcon faceplate were read out, and the charge representing the brightness of individual pixels was digitized into 0–255 levels. This digitization represented the fundamental dynamic range of the cameras, thus all information from overexposed pixels was lost. The dynamic range could be effectively extended through multiple exposures, having a range of exposure times. The photometric linearity of the images was established though the use of a series of stepped calibration images of the UV flood lamps, having different exposure times. These calibration images sampled the dynamic range of the camera as a linear function of photometric intensity such that linearized science images could then be formed by interpolation with respect to the sets of calibration images. The detector image was corrected for geometrical distortions though the use of a grid of reseau marks etched onto the detector faceplate. Spectral data coinciding with these reseau marks were not reliable. In addition, each camera possessed a slightly different response to the operational temperature of the detector (the camera head amplifier temperature, or THDA), as well as time-dependent sensitivity drifts which manifested themselves as general declines in sensitivity throughout the mission. All *IUE* data processing systems corrected for these effects, to first order, but improvements to the data processing procedures continued throughout the mission.

Low-dispersion spectra produced a single linear trace on the detector. For a point source, the extraction of the corresponding one-dimensional spectrum involves the subtraction of the non–sky detector background and a mapping of the flux pixels onto a physical wavelength scale. Spectra extracted in "trailed," or multiple exposure modes have slightly different calibration characteristics. The final step was to photometrically calibrate the spectra using an absolute instrumental sensitivity derived from observations of a set of spectrophotometric standard calibration stars. A detailed description of *IUE* data and data reduction procedures is contained in Garhart et al. (1997).

1.2. *NEWSIPS Data*

Due to its long operational lifetime and the strong involvement of an active observer community, understanding of the behavior of the *IUE* cameras evolved greatly over time. The net result was a steady improvement in the quality of the spectra, which could be extracted from *IUE* images using different generations of the data reduction system. Near the end of *IUE* operations, it was decided to reprocess all images in a uniform fashion using a final version of the data reduction software called NEWSIPS. NEWSIPS procedures and its associated data products are described in NL96. Briefly, among the more important improvements realized with NEWSIPS are (1) better definition of the fixed pattern noise in the cameras, (2) better geometrical correction of the images, including a transformation the axes of the large apertures so they are orthogonal to the line and sample axes, (3) better definition of the intensity transfer function for each camera, which enhances the photometric linearity of the spectra, (4) improved point source extraction procedures based on optimal extraction, and (5) an improved absolute calibration defined with respect to a model atmosphere spectrum of the hot white dwarf G191-B2B. NL96 document a 10%–50% improvement in NEWSIPS spectral S/N for single images, depending on the camera and observing conditions. In particular, the improved treatment of fixed pattern noise makes possible a much steeper increase in S/N as a function of the number of co-added spectra. NEWSIPS data resulted in several new output file formats. Of particular interest to the archive discussed in this paper are the "MXLO" (Low-Dispersion Extracted Image FITS Files) files which contain extracted spectra, uncertainty vectors, and data flags for extracted one-dimensional spectra. In summary, NEWSIPS data represent the baseline standard for *IUE* data, for most applications.

1.3. *Massa-Fitzpatrick Corrections*

Although, NEWSIPS data achieved a significant advance over earlier *IUE* data reduction schemes, the final scope of this effort was ultimately limited by time, resources, and the need for a single general data reduction process that worked well for all classes of objects and spectra. There remain residual instrumental and data reduction effects that persist in NEWSIPS data. Massa & Fitzpatrick (2000, hereafter MF00) provide a detailed description of how these effects manifest themselves in individual cameras and observing modes.

In particular, MF00 identified residuals in NEWSIPS spectra that are separately correlated with long-term temporal variations and with thermal effects (THDA). A further significant change to the NEWSIPS data involved the adoption of the *Hubble Space Telescope* (*HST*) Faint Object Spectrograph (FOS) absolute flux scale (Bohlin 1996). (It should be noted that because of the way in which the MF00 corrections are defined and applied, the transfer from NEWSIPS to *HST* flux scales cannot be consistently defined for all uncorrected NEWSIPS spectra but must be applied to MF00 corrected spectra.) In addition, MF00 made small but important corrections to the wavelength scale of the LWR and LWP spectra. MF00 conveniently addressed all of these residual effects by developing a series of corrections that are particularly optimized for low-dispersion spectra of hot continuum sources. Since the vast majority of white dwarfs observed with *IUE* easily fit this description, we have adapted the MF00 corrections in processing our archive spectra. MF00 demonstrate that application of these corrections can lead to noise levels which approach the 3% of the signal for optimally exposed images. Moreover, compensation for the temporal and thermal effects also leads to a significant increase in the repeatability observed in spectra of the same star which were obtained over the span of the mission. This directly translates into a further useful gain in the S/N of co-added spectra.

The MF00 corrections operate on the extracted "MXLO" NEWSIPS spectra and are defined for all common combinations of SWP, LWP, and LWR cameras, observing modes (point, trailed, or multiple exposure) and apertures (LAP and SAP). The original routines and files to perform these corrections were kindly supplied by Derek Massa. For our purposes, we incorporated these corrections into a single IDL (Interactive Data Language) procedure that produced fully corrected spectra. In Figure 1 we illustrate the application of MF00 corrections to NEWSIPS spectra followed by co-addition for the white dwarf HZ 43.

1.4. *Improved Signal-to-Noise*

One of the major motivations for undertaking the construction of this archive of *IUE* low-dispersion spectra was the opportunity to make a significant improvement to the overall S/N of the spectra through application of the MF00 corrections together with further improvements, where it was possible to co-add multiple spectra.

Because the MF00 corrections improve the reproducibility of *IUE* spectra, the co-addition of spectra can significantly improve S/N. In Figure 2 we plot the empirically measured S/N as a function of the number of spectra co-added. The data are for SWP and LWR/LWP large aperture spectra of the hot DA white dwarf WD 0501+527 (G191-B2B) and represent respective measurements of S/N over the wavelength ranges 1350 to 1450 Å and 2200 to 2400 Å. The dotted and solid curves in Figure 2, respectively, represent the expected $\sqrt{N_{\rm spectra}}$ increase in S/N with the co-addition of up to 15 SWP and LWR/LWP spectra. As is evident, there is little advantage in co-additions that exceed 10 or 12 spectra. As a practical matter, it was therefore decided to limit the number of spectra co-added to not more than 10 or 12, even if additional spectra existed.

1.5. *Absolute Calibration*

All NEWSIPS spectra were flux calibrated (NL96) based on a synthetic model atmosphere energy distribution for the star G191-B2B (WD 0501+527). This definition of the absolute flux scale currently differs both in level and wavelength dependence in subtle ways from the absolute flux scale in use for *HST* (see MF00 for a discussion of this issue). Among the corrections applied to the NEWSIPS data by MF00 was to place the absolute fluxes for the three cameras (SWP, LWP, LWR) on the *HST* FOS scale defined by Bohlin (1996). We follow this procedure and use this flux scale. An example of the application of this flux scale is shown in Figure 3, where our co-added spectrum for the star GD 71 (WD 0549+158) is compared with a model replicating the Bohlin flux for GD 71.

The co-added GD 71 spectrum shown in Figure 3 consists of 10 SWP (eight LAP and two SAP) and nine LWP/LWR spectra (eight LWP and one LWR). As is evident from the plot of the relative residual flux (*observed/model-1*) in Figure 3, the SWP region is characterized by sample-to-sample fluctuations below the ±3% level. There are some indications of low-frequency wavelength dependence; however, very little of this correlates well with similar plots for other stars (GD 659, GD 246, HZ 43, and G191-B2B). In the long-wavelength region residuals are higher, with sample-to-sample fluctuations at ±7%. In addition, there is a tendency for fluxes longward of 2500 Å to be approximately +3% too high with respect to the model. The latter aspect of the data is seen in other stars as well. In summary, the combination of MF00 corrections and co-addition demonstrate an excellent match to the *HST* FOS flux scale and exhibit an S/N which approaches 50:1.

As has been noted (see Holberg et al. 1982, 1991, Finley et al. 1997, and Bohlin, Colina, & Finley 1995) hydrogen-rich (DA) white dwarfs have a number of advantages as absolute flux standards. Among these advantages are strong, almost featureless, UV continua, and a general lack of any detectable interstellar reddening. The major advantage, however, is the ability of relatively unambiguous model atmosphere calculations to fully represent not only the overall energy distributions of these stars but also their detailed line profiles. The high confidence in such representations is principally a result of the fact that only hydrogen opacities are involved in the models. In principle, only the effective temperature ($T_{\rm eff}$) of the star, its surface gravity ($\log g$), and a monochromatic flux normalization (usually V magnitude) need to be established to fully define the observed flux at the top of Earth's atmosphere. All of these quantities can be determined, independently from the UV stellar energy distribution, through a careful analysis of the H I Balmer profiles together with an accurate V magnitude.

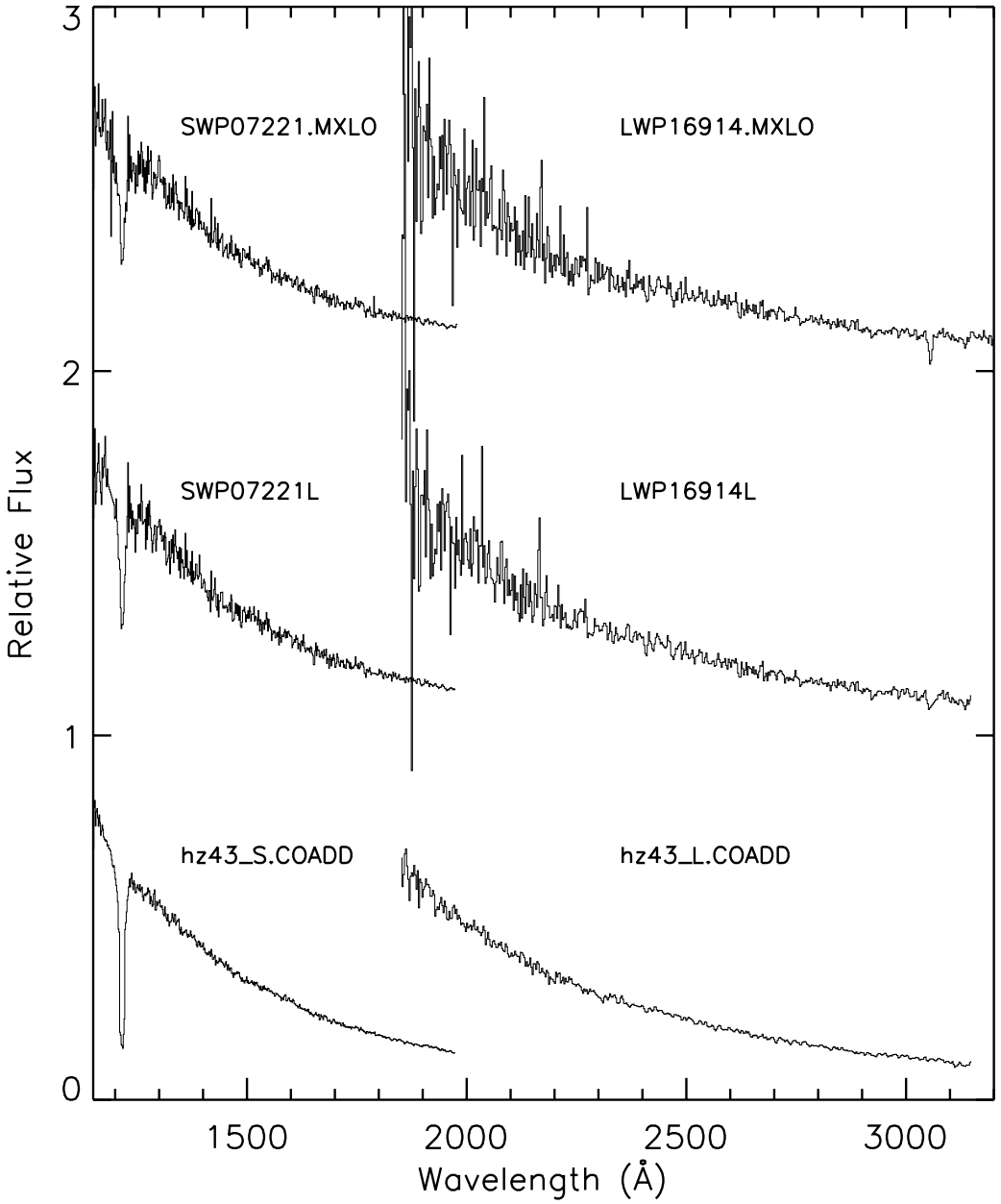

FIG. 1.—Comparison of a sequence of NEWSIPS and MF00 corrected spectra for the white dwarf WD 1314+293 (HZ 43). The upper spectra are individual SWP and LWP NEWSIPS spectra, the middle spectra are the MF00 corrected versions of the same spectra. The bottom spectra are the corresponding co-added short- and long-wavelength spectra.

2. DATA REDUCTION PROCEDURES

2.1. *Processing of the IUE Spectra*

For our archive of the white dwarfs, processing of the *IUE* low-dispersion spectra begins with the extracted NEWSIPS "MXLO" spectra obtained from the Multimission Archive at STScI (MAST). The MF00 corrections are performed on the MXLO spectra using an IDL procedure that applies all of the corrections in a single pass. The resulting output spectra are resampled onto standard wavelength scales for each camera, and a flux uncertainty vector and custom data flag vector are constructed. The final, fully corrected spectra are then written to an internal IDL save file. All NEWSIPS spectra for a given star are processed in a batch mode which also initiates a cumulative log file that controls subsequent data processing and records a processing history for the spectra associated with each star. Critical input information such as the camera, aperture, exposure time, exposure mode (point, trailed, or multiple exposure), and extraction method (point or extended source) are obtained from the spectral header and written to the associated log file. At this stage, individual spectra are also plotted and inspected for any problems or anomalies.

Subsequent processing of the set of spectra associated with each star depends on the nature of the data set of spectra for that star. If only a single SWP or LWP/LWR spectrum exists, no further processing is conducted and a final spectrum with a suffix "CORR," indicating application of MF00 corrections, is saved. If, however, multiple spectra exist, then these may be co-added. The co-addition

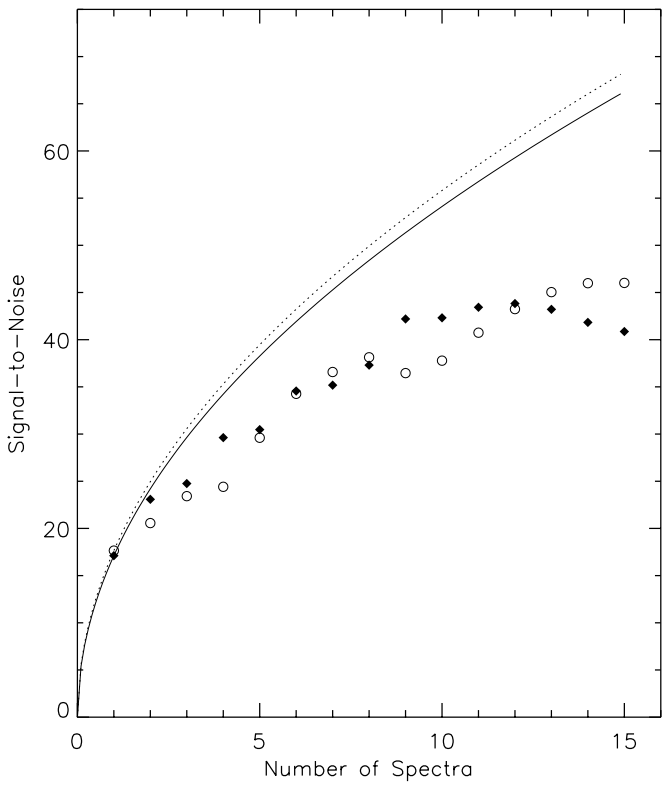

FIG. 2.—Measured signal-to-noise ratio as a function of the number of co-added spectra for G191-B2B. The open circles represent SWP spectra for the wavelength range 1350 to 1450 Å. The filled diamonds represent LWP/LWR spectra for the wavelength range 2200 to 2400 Å. The dashed and solid curves represent the expected idealized $\sqrt{N}$ dependence for the SWP and LWP/LWR spectra, respectively.

process is similar to that described in Barstow et al. (1997). Individual spectra are ratioed and median flux ratios determined for wavelength ranges free of strong spectral features (i.e., Lyα), overexposed or poorly exposed regions, reseau marks and blemishes. For large aperture spectra, these ratios are expected to be near 1.0. If for some reason a large aperture spectrum exhibits a ratio significantly different from 1.0 or has a spectral ratio with strong wavelength dependence, then it is either excluded from the co-addition process or a questionable wavelength region, for example, an unflagged cosmic-ray hit or a blemish can be flagged "bad." For small aperture spectra, spectral ratios near 1.0 are not necessarily expected, since light is lost through this aperture and the flux levels of the spectrum are a function of the instrument focus and the placement of the stellar image. The unattenuated flux for a small aperture spectrum can usually be determined from any existing large aperture spectra of the same star, through an examination of the large to small aperture flux ratios. For example, it is frequently the case that a star has several large aperture spectra and perhaps one small aperture spectrum. In such cases, the large aperture spectra are ratioed to the small aperture spectrum and the median of each flux ratio is determined over a portion of the spectrum which is reasonably flat, usually between 1350 and 1650 Å. The resulting medians are then averaged to define the factor by which the small aperture spectrum is to be multiplied during the co-addition process.

The co-addition process itself is controlled by a set of scale factors and excluded wavelength regions that are predefined in the log file. A weighted mean co-added spectrum is automatically formed, under control of the log file, by application of these scale factors and wavelength exclusion regions. Provision for linearly shifting the wavelength scale of a spectrum exists but was not used in any of the low-dispersion spectra in this archive. Wavelength regions excluded during co-addition are assigned zero weight. In most instances, excluded wavelength regions were used to control the co-addition of spectra in the Lyα region, near 1216 Å, so that only those spectra having the lowest level of geocoronal contamination were used. A good example of the co-addition procedure is shown in Figure 4, where an annotated portion of the log file used to define the co-addition of the star GD 659 (WD 0050−330) is shown.

A co-added spectrum is the weighted mean of its component spectra. Weighting is proportional to the exposure time for each spectrum. Additionally, a point-by-point Gaussian weighting with respect to the uncertainty vector is also applied. A net co-added uncertainty vector that reflects the resulting S/N of the co-added flux vector is also computed. Flux pixels corresponding to overexposed regions, reseau marks, cosmic-ray hits, or similar artifacts flagged by the NEWSIPS processing, are assigned a flag of 0. Otherwise, flux pixels are assigned a flag of 1. During co-addition, pixels flagged with 0 are effectively excluded from the co-added result. A final co-added flag vector can have values intermediate between 0 and 1, which reflect the proportion of valid pixels which were co-added. In the case of LWP and LWR spectra, they are co-added using a common wavelength scale since the MF00 corrections effectively diminish the distinctive differences between these two cameras.

The resulting co-added spectra are written as IDL save files with a suffix denoting the name of the star and an "S" for short wavelength or an "L" for long wavelength and an appended suffix "COADD." In the example shown in Figure 4, the co-added short- and long-wavelength spectra are assigned filenames "gd659_S.COADD" and "gd659_L.COADD," respectively. A further concatenation step in which the long- and short-wavelength spectra are combined into a single spectrum with a wavelength range from 1150 to 3200 Å is applied for stars having both "L" and "S" spectra. For example, in Figure 4 the "gd659_S.COADD" and "gd659_L.COADD" are concatenated into a single spectrum called "gd659.CONCAT." The overlap region between SWP and LWP/LWR spectra are resampled onto the SWP wavelength scale, and a common weighted flux is computed. In most instances this results in a seamless joining of the two spectral regions with no artifacts or significant changes in flux level.

2.2. *Log Files*

Associated with each spectrum is a log file which indicates, among other things, which spectra were co-added and combined to produce the final spectrum and exactly how the co-addition was implemented. Users of this archive are encouraged to consult these log files since they contain valuable information on how the final spectra were produced. An example of a log file is shown for the white dwarf GD 659 (WD 0050−330) in Figure 4. The first stage is a record of the SWP, LWP, and LWR NEWSIPS files that are associated with each star and their unique filenames. Plots of each spectrum were visually evaluated for any obvious problems. Comments on individual spectra—for example,

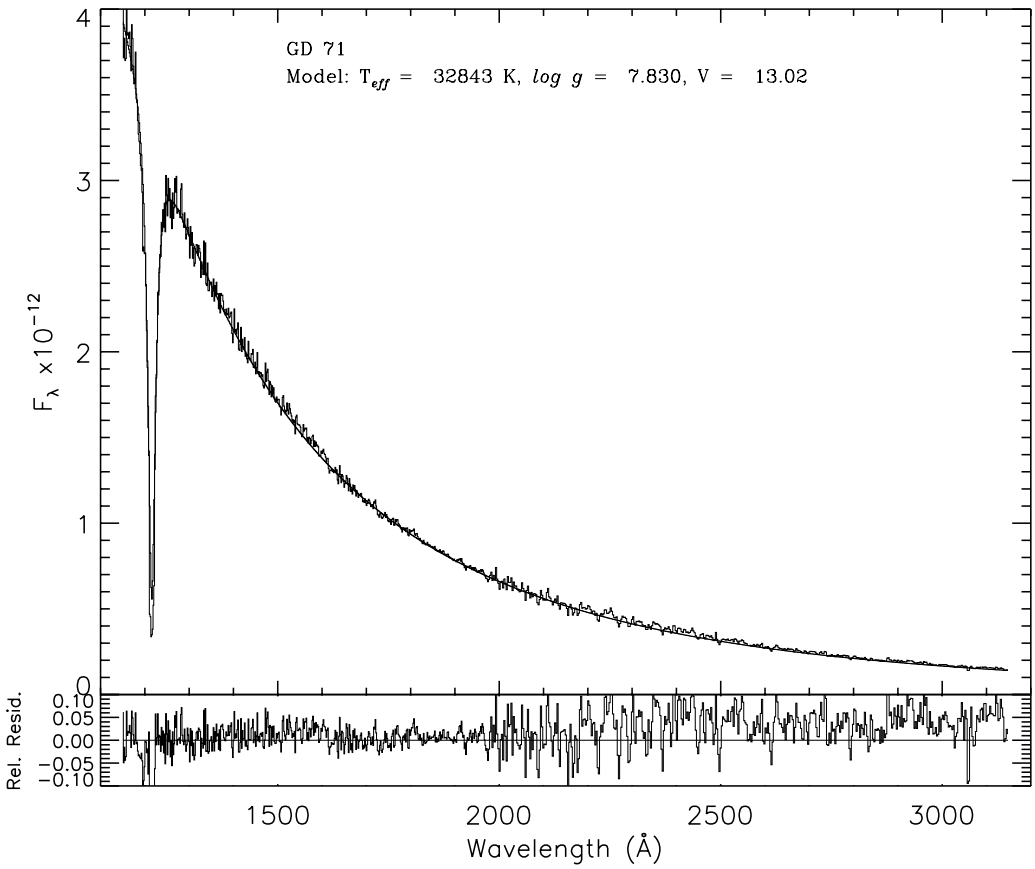

FIG. 3.—Comparison of the archive spectrum of GD 71 with a model replicating the *HST*-FOS absolute flux for GD 71 (Bohlin 1996). No adjustment has been made to the model to match the observed fluxes. The bottom panel shows the relative residual spectrum (*observed/model-1*).

obvious problems with the flux level, or even the lack of an apparent signal—are noted here. This stage also contains the name of the MF00 corrected file which is saved as an IDL file; the file name contains the image ID together with an "L" or "S" for large or small aperture, respectively. Also included is information from the NEWSIPS spectral header including the extraction mode ("EXTENDED" or "POINT"), an indication of the "X-OFFSET" of the spectrum, an indication of whether or not the spectrum was trailed, an indication of whether the exposure was segmented in time, and the total exposure time in seconds. The mode of the spectrum is also given. The second stage indicates the spectral ratios that were produced and examined as a check on the mutual agreement of the flux levels for the set of spectra. This step was also used to determine the scale factors for the SWP small aperture spectra as well as to determine the extent of the wavelength region bracketing Lyα to be excluded. In general, a single spectrum was chosen to ratio with all the other spectra. If available, the spectrum chosen for this task was a small aperture spectrum. In such cases, the level of the ratio provides information on the scale factor by which that particular small aperture spectrum will be multiplied during the co-addition process. If no useful small aperture spectrum was available, a well-exposed large aperture spectrum was ratioed with all the others; the expectation being that the resulting ratios should be near 1.0. A similar set of ratios was produced for all LWR and LWP spectra. This process easily identifies spectra with obvious flux level differences. The third stage of the log file defines the factors used to control the co-addition process, such as the exposure time of the image, the wavelength shift (always zero), the scale factor, the exposure times of the images and the Lyα wavelength region flagged for exclusion during co-addition. If the region of excluded wavelengths falls outside the wavelength limits of the spectrum, then no action is taken and all wavelengths are included in the co-addition. This allows the Lyα region of the final co-added spectrum to be represented only by those spectra having the lowest relative level of geocoronal contamination. As mentioned previously, such spectra are often the small aperture spectra. The file names for the co-added spectra are assigned at this point. The fourth and final stage of the log file controls how the final files are produced. If short- and long-wavelength spectra exist, then a final concatenated file is produced with the suffix "CONCAT." If only a short- or long-wavelength file exists, then the file suffix is "COADD." If no co-addition was preformed, then the corresponding suffix is "CORR" since only MF00 corrections were applied.

All final spectra consist of four vectors, namely a wavelength vector, a flux vector, an uncertainty vector, and a status flag vector. In Table 1 the wavelength limits and sampling used for the several varieties of output files are presented.

3. THE WHITE DWARF ARCHIVE

The objects contained in this archive were selected primarily on the basis of the standard user-assigned classifications in the *IUE* Merged Log that correspond to white

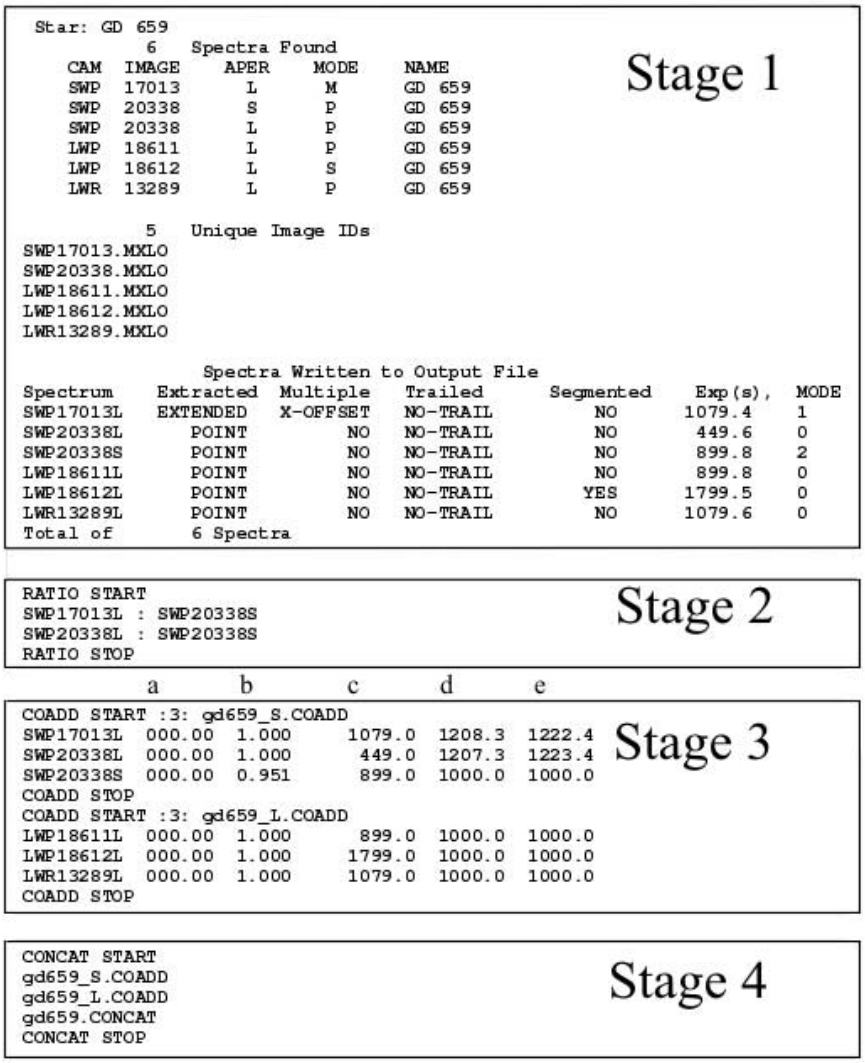

FIG. 4.—Example of a log file for the star GD 659. The processing stages are explained in the text.

dwarfs. Additional observations of binary systems where the original target was not necessarily the white dwarf are also included. An effort was made to include known white dwarfs, even if they were not classified as such by the original observers. In general, central stars of planetary nebulae were not included unless they were also contained in the McCook & Sion (1999, hereafter MS99) catalog of white dwarfs. Some observed spectra do not contain any apparent continuum source, perhaps due to intrinsic faintness in the UV or because the target was not in the slit. These observations are included for the purposes of completeness, but the lack of signal has been noted in the associated log file. The contents of the archive are summarized in Table 2, which contains the MS99 white dwarf number for each star, an alternate name, the spectral type, the number of spectra for each camera and aperture that were co-added, and a total of the number for a given star. Note that the total number of spectra represents all existing spectra for each star and may exceed the number used for co-addition (see § 3.1). The IDL files mentioned in this paper are internal to the data reduction effort but are available upon request from J. B. H. The final data files, log files, and plot files for all stars in Table 2 are available on-line (see acknowledgements). The data are available either as ASCII tables or as FITS files.

TABLE 1

WAVELENGTH SCALES FOR ARCHIVE OUTPUT FILES

File Type	W_{min} (Å)	W_{max} (Å)	$\Delta\lambda$ (Å)	Number Points
.CONCAT	1150.58	3148.50	1.6764 (2.6690)	933
_S.COADD	1150.58	1973.67	1.6764	492
_L.COADD.....	1851.42	3148.50	2.6690	487
_S.CORR	1150.58	1973.67	1.6764	492
_L.CORR	1851.42	3148.50	2.6690	487

3.1. *Anomalous Spectra*

The process of correcting and co-adding the NEWSIPS spectra encountered few difficulties. Nevertheless, a number of anomalous observations and spectra were noted in the log files. These tended to fall into several categories.

LWP streak.—Several stars in the archive display clear evidence of contamination by scattered sunlight at long wavelengths. Often referred to as the "LWP streak," this

TABLE 2

WHITE DWARFS IN THE LOW-DISPERSION *IUE* ARCHIVE

WD NUMBER	ALT. ID	SPECTRAL TYPE	SWP		LWP/LWR		TOTAL
			LAP	SAP	LAP	SAP	
WD 0000−170	LTT 11	DB4	1	...	1	...	2
WD 0002+729	GD 408	DBZ4	1	1	1	...	3
WD 0004+330	GD 2	DA1	2	1	1	...	4
WD 0005+511	KPD0005+5106	DOZ	2	...	...	...	2
WD 0017+136	Feige 4	DB3	2	...	1	...	3
WD 0022−745	HD 2133B	DA1+F8 V	2	...	1	...	3
WD 0037+312	GD 8	DA1	1	1	2	...	5
WD 0038+555	G218−8	DQ5	1	...	1	...	2
WD 0041+092	RE J0044+093	DA2+K0 IV	2	...	1	...	3
WD 0041−102	Feige 7	DAP2	2	...	1	...	3
WD 0044−121	NGC 246	PNN	9	1	10	...	34
WD 0046+051	van Maanen 2	DZ7	...	...	2	...	3
WD 0046+077	PG 0046+078	DO.7	1	...	1	...	2
WD 0047−524	BPM 16274	DA2	7	...	7	...	14
WD 0050−332	GD 659	DA1.5	2	1	3	...	6
WD 0100−068	G270−124	DB3	1	1	2	...	5
WD 0101+048	G2−17	DA6	1	...	1	...	2
WD 0101−182	MCT 0101−1817	DO	1	...	1	...	2
WD 0104−464	BPM 30551	DAV	1	...	...	...	1
WD 0108+100	PG 0108+101	DOZ.6	1	...	1	...	2
WD 0109+111	PG 0109+111	DOZ.7	1	...	1	...	2
WD 0109−264	GD 691	DA1	2	1	1	...	4
WD 0112+104	PG 0112+104	DB1.6	4	3	2	...	9
WD 0114−027	HD 7672	DA3+G5 III	9	1	2	...	12
WD 0115+159	G033−049	DQ5	2	...	1	...	3
WD 0122+200	PG 0122+200	DOZ.7	2	...	...	...	2
WD 0128−387	MCT 0128−3846	DAB	2	...	1	...	3
WD 0130−196	MCT 0130−1937	DO.5	3	1	1	...	5
WD 0131−163	GD 984	DA1	3	...	2	...	8
WD 0133−116	ZZ Ceti	DAV	1	...	...	...	5
WD 0134+181	PG 0134+181	DAO1	1	...	...	...	1
WD 0134+833	GD 419	DA2.5	3	1	1	...	5
WD 0135−052	L870−2	DA7	2	...	2	...	4
WD 0136+251	PG 0136+251	DA1	2	...	1	...	3
WD 0141−675	LFT 158	DA7	1	...	3	...	5
WD 0145−257	GD 1401	DA2	2	...	1	...	3
WD 0148+467	GD 279	DA3.5	2	...	2	...	4
WD 0200−127	GD 1072	DC	1	...	1	...	3
WD 0205+250	G35−29	DA2.5	1	...	...	...	1
WD 0209+085	HS 0209+0832	DAB1.4	2	...	1	...	3
WD 0214+568	H Per 1166	DA2	2	1	...	...	3
WD 0216+143	PG 0216+144	DA2	1	...	1	...	2
WD 0226−615	HD 15638	DA1+F6 V	3	...	1	...	4
WD 0227+050	Feige 22	DA2.5	2	...	1	...	3
WD 0229−481	LB 1628	DA1	1	...	...	...	1
WD 0231−054	GD 31	DA6	1	...	...	...	1
WD 0232+035	Feige 24	DA+dM1	7	5	2	...	16
WD 0232+525	G174−5	DA3	1	...	...	...	1
WD 0237+115	PG 0237+116	DO1	1	...	1	...	2
WD 0250−026	KUV 02503−0238	DA	1	...	1	...	2
WD 0252−055	HD 18131B	DA1.5	1	...	1	...	2
WD 0255−705	BPM 2819	DA6	3	...	3	...	6
WD 0300−013	GD 40	DB3	1	...	2	...	3
WD 0302+027	Feige 31	DA1.5	3	...	1	...	5
WD 0308+096	PG 0308+096	DA4	1	...	...	...	1
WD 0308−565	BPM 17088	DB3	1	...	1	...	2
WD 0310−688	LB 3303	DA3	1	...	1	...	2
WD 0316−849	RE J0317−853	DA1H	4	...	2	...	6
WD 0320−539	LB 1663	DA1.5	2	1	1	...	4
WD 0343−007	KUV 0343−007	DA1	1	...	1	...	2
WD 0346−011	GD 50	DA2	5	4	3	...	12
WD 0347+171	V471 Tau	DA1.5+K2 V	8	1	6	...	33
WD 0348+339	GD 52	DA4	1	...	...	...	1

TABLE 2—*Continued*

WD Number	Alt. ID	Spectral Type	SWP		LWP/LWR		Total
			LAP	SAP	LAP	SAP	
WD 0352+096	HZ 4	DA4	3	...	4	...	9
WD 0353+284	RE J0357+283	DA2.5+K2 V	1	...	1	...	2
WD 0354−368	MS 0354.6−3650	DA1+G2 V	1	...	...	...	1
WD 0401+250	G8−8	DA4	1	...	1	...	2
WD 0406+169	LB 227_ver 1	DA4	5	...	7	...	17
WD 0406+169	LB 227_ver 2	DA4	5	...	5	...	17
WD 0410+117	HZ 2	DA2.5	5	...	6	...	11
WD 0413−077	40 Eri B	DA3	5	2	3	...	10
WD 0416−550	WD 0416−551	DA1.5	1	...	1	...	2
WD 0418+137	HD 27483	DA3+F6 V	2	1	...	...	3
WD 0418−539	BPM 17731	DB3	1	...	1	...	2
WD 0421+336	HD 27786	DA3+F4 V	3	1	2	...	6
WD 0421+740	RE J0427+741	DA1	1	...	...	...	1
WD 0425+168	EG 37	DA2	1	...	1	...	2
WD 0426+588	G175−34B	DQ7	1	...	1	...	4
WD 0429+176	HZ 9	DA2.5+dM4e	1	1	1	...	3
WD 0441+467	S 216	DAO	3	...	2	...	5
WD 0453−295	MCT 0453−295	DAB3	4	...	2	...	6
WD 0453+418	GD 64	DA3.5	1	...	1	...	2
WD 0455−282	RE J0457−280	DA1	4	...	2	...	8
WD 0457−103	HD 32008B	DA2+K0 IV	2	...	1	...	3
WD 0458−364	RE J0500−362	DA1+F6 V	2	...	...	...	3
WD 0500−156	Abell 7	DAO	3	1	3	...	12
WD 0501+527	G191−B2B	DA1	10	2	12	...	115
WD 0501−289	RE J0501−289	DO.7	3	...	3	...	6
WD 0504−241	WD 0504−241	DO.7	1	...	1	...	2
WD 0507+045	HS0507+0435A	DA4.5	1	...	...	...	1
WD 0509−007	RE J0512−004	DA2	1	1	...	...	2
WD 0511−230	0511−230	DA?	1	...	1	...	2
WD 0512+326	KW Aur C	DA1.8+F4 V	4	...	1	...	6
WD 0517+307	GD 66	DAV4	1	...	...	...	1
WD 0518−105	RE J0521−102	DA2	1	...	...	...	2
WD 0531−022	RE J0534−021	DA2	1	...	...	...	2
WD 0548+000	GD 257	DA1	2	1	2	...	9
WD 0549+158	GD 71	DA1.5	8	2	9	...	19
WD 0612+177	EG 46	DA2	5	4	1	...	11
WD 0615+655	HS 0615+6535	DA.51	...	1	1	...	4
WD 0615−591	BPM 18164	DB4	2	...	2	...	4
WD 0621−376	RE J0623−374	DA1	3	1	...	...	4
WD 0631+107	WD 0631+107	DA2	1	1	...	...	2
WD 0644+375	EG 50	DA2.5	2	1	1	...	4
WD 0646−253	RE J0649−252	DA2	1	...	...	...	1
WD 0651−020	GD 80	DA1.5	2	1	...	...	3
WD 0659+130	RE J0702+125	DA1.5+K0 IV	1	...	2	...	3
WD 0704+618	HS 0704+6153	DO.8	1	...	...	...	2
WD 0713+399	HS 0713+3958	DO.7	2	...	1	...	3
WD 0714+458	GD 84	DBA6	1	...	...	...	1
WD 0715−703	RE J0715−702	DA1	1	...	...	...	1
WD 0718−316	RE J0720−318	DAO1+dM5e	2	...	1	...	4
WD 0727+600	HS 0727+6003	DO.6	1	...	...	...	1
WD 0738−172	L745−46A	DZQ6	1	...	2	...	3
WD 0742+653	HS 0742+6520	DOZ.6	1	...	...	...	1
WD 0802+413	KUV 343−6	DA1	1	1	1	...	3
WD 0806−661	L97−3	DQ4	1	...	1	...	2
WD 0823+316	PG 0823+317	DAO.5	2	1	...	...	3
WD 0824+288	PG 0824+289	DA1+dC	5	1	3	...	9
WD 0830−535	RE J0831−534	DA1.7	1	...	...	...	1
WD 0836+237	PG 0836+237	DA2	2	...	...	...	3
WD 0839−327	EG 62	DA5.3	1	...	1	...	3
WD 0840+262	TON 10	DB3	1	...	1	...	2
WD 0845−188	LDS 235B	DB4	4	...	2	...	6
WD 0846+249	PG 0846+249	DAO	3	...	...	...	3
WD 0853+163	PG 0853+163	DBP2	1	...	1	...	3
WD 0858+363	GD 99	DAV	2	...	1	...	3

TABLE 2—*Continued*

WD Number	Alt. ID	Spectral Type	SWP		LWP/LWR		Total
			LAP	SAP	LAP	SAP	
WD 0904+511	PG 0904+512	DA1.5	1	...	...	...	1
WD 0905−724	HD 78791	DA1.5+F9 II	2	...	1	...	3
WD 0912+536	G195−19	DXP7	1	...	1	...	2
WD 0921+091	PG 0921+091	DB2	1	...	...	...	1
WD 0921+354	G117−B15A	DAV4	2	...	...	...	2
WD 0930+815	HD 81817	DA3+K3 IIIa	2	...	...	...	3
WD 0935−371	LDS 275AB	DA5	1	...	1	...	2
WD 0939+262	PG 0939+262	DA0.5	2	2	2	...	7
WD 0943+441	G116−52	DA3	1	...	1	...	2
WD 0945+245	PG 0945+246AB	DA3	3	...	1	...	4
WD 0947+857	RE J0957+852	DA1	1	...	...	...	1
WD 0948+013	PG 0948+013	DB2	1	...	...	...	1
WD 0950+139	PG 0950+139	DA0.5	3	...	...	...	3
WD 0954−710	BPM 6082	DA5	1	...	1	...	2
WD 1003−441	Lo 4	PG 1159	2	...	...	...	2
WD 1010+064	PG 1010+065	DA1	1	...	1	...	2
WD 1011+570	GD 303	DBZ4	1	...	1	...	2
WD 1013−050	RE J1016−053	DAO1+dM5e	4	...	1	...	5
WD 1015+014	PG 1015+014	DA3.5	1	...	...	...	1
WD 1021+266	BD+27 1888B	DA1.5+F0 V	3	...	1	...	4
WD 1022+050	LP 550−52	DA4.5	1	...	1	...	2
WD 1024+326	RE J1027+322	DA1.5+GV	2	...	...	...	2
WD 1026+002	PG 1026+002	DA4.5	1	...	...	...	1
WD 1026+453	PG 1026+454	DA1.5	1	...	...	...	1
WD 1031+234	PG 1031+234	DA3.5	1	...	1	...	2
WD 1031−114	EG 70	DA2	2	1	...	...	3
WD 1033+464	GD 123	DA1.5+dK	2	1	...	...	3
WD 1034+001	PG 1034+001	DOZ.5	9	...	6	...	17
WD 1041+580	PG 1041+580	DA1.5	1	...	...	...	1
WD 1042−690	BPM 6502	DA2.5+dM	1	...	1	...	2
WD 1052+273	GD 125	DA2	2	1	...	...	3
WD 1053−550	LTT 4013	DA5	1	...	...	...	1
WD 1055−072	LHS 2333	DA7	1	...	1	...	2
WD 1056+516	LB 01919	DA1	1	...	...	...	1
WD 1057+719	PG 1057+719	DA1	1	1	...	...	2
WD 1057−059	PG 1057−059	DO1	1	...	...	...	1
WD 1104+602	WD 1104+602	DA3	1	...	1	...	2
WD 1105−048	L970−30	DA3	1	...	1	...	2
WD 1108+325	PG 1108+325	DA1	1	...	...	...	1
WD 1109+244	PG 1109+244	DA1.5	1	...	2	...	3
WD 1109−225	HR 4343	DA1.5+A1 V	3	2	...	...	5
WD 1115+158	PG 1115+158	DBV2	1	...	1	...	2
WD 1116+026	PG 1116+026	DA3.5	1	...	...	...	1
WD 1121+145	PG 1121+145	DA	1	...	1	...	2
WD 1123+189	PG 1123+189	DA4	1	1	1	...	4
WD 1133+489	PG 1133+489	DO1	2	...	1	...	1
WD 1134+300	GD 140	DA3	2	1	2	...	5
WD 1142−645	L145−141	DQ6	2	...	3	...	5
WD 1143+321	G148−7	DA3.3	1	...	...	...	1
WD 1144+004	PG 1144+005	DO1	2	1	...	...	3
WD 1149−133	PG 1149−133	DB2	1	...	1	...	2
WD 1151−029	PG 1151−029	DOZ1	2	...	1	...	3
WD 1159+803	G255−2	DAV	1	...	...	...	1
WD 1159−034	PG 1159−035	DQZO.4	9	...	7	...	19
WD 1202+608	Feige 55	DAO + wd	1	1	2	...	4
WD 1210+533	PG 1210+533	DAO1	2	1	1	...	4
WD 1211+332	HZ 21	DO1	9	...	7	...	35
WD 1211−169	HE 1211−1707	DAH	2	...	...	...	2
WD 1225−079	K 789−37	DZ5	1	...	1	...	2
WD 1234+481	HS 1234+4811	DA1	2	1	2	...	5
WD 1236−495	LHS 2594	DA6	1	...	1	...	2
WD 1239+481	PG 1234+482	DA1	2	1	2	...	5
WD 1253+261	RE J1255+255	PNN	1	...	...	...	1
WD 1253+378	HZ 34	DAO1	1	...	1	...	3

TABLE 2—*Continued*

WD Number	Alt. ID	Spectral Type	SWP		LWP/LWR		Total
			LAP	SAP	LAP	SAP	
WD 1254+223	GD 153	DA1.3	10	1	10	...	22
WD 1302+597	GD 323	DAB1.7	2	1	1	...	4
WD 1305−017	PG 1305−017	DAO1	1	...	...	...	1
WD 1307+354	GD 154	DA4.5	1	...	...	...	3
WD 1311+129	PG 1311+129	DBA3.3	1	...	1	...	2
WD 1312+098	PG 1312+099	DCP3.4	1	...	1	...	2
WD 1314+293	HZ 43	DA1	7	3	6	2	23
WD 1326−037	PG 1326−037	DB2	1	...	1	...	2
WD 1327−083	Wolf 485	DA4	12	...	12	...	51
WD 1333+487	GD 325	DB	1	1	1	...	4
WD 1337+705	EG 102	DA3	10	1	9	...	20
WD 1347−129	EC13471−1258	DA+dM	1	...	...	...	2
WD 1351+489	PG 1351+489	DBV2	1	...	1	...	2
WD 1403−077	PG 1403−077	DA1.5	1	...	...	...	1
WD 1411+218	PG 1411+219	DB4	1	...	1	...	2
WD 1413+015	PG 1413+015	DAO	1	...	...	...	1
WD 1413+231	PG 1413+232	DA2	1	...	...	...	1
WD 1424+534	PG 1424+535	DOQZ.5	2	...	2	...	4
WD 1425+540	G200−039	DBAZ4	1	1	...	...	2
WD 1425−811	L19−2	DA6	1	...	1	...	4
WD 1445+152	PG 1445+153	DB2	2	...	2	...	4
WD 1456+103	PG 1456+103	DBV	1	...	1	...	2
WD 1459+821	G256−018	DB4	1	...	1	...	2
WD 1501+664	H 1504+65	DZ1	2	1	2	...	7
WD 1517+740	HS 1517+7403	DO.5	1	...	1	...	2
WD 1520+525	PG 1520+525	DOQZ.4	2	1	1	...	4
WD 1532+033	PG 1532+033	DA.5	1	1	...	...	2
WD 1542+182	GD 190	DB3	2	...	1	...	3
WD 1544+009	BD 1 3129A	DA	1	...	...	...	1
WD 1544−377	L481−060	DA5	3	...	2	...	5
WD 1548+405	PG 1548+405	DA1	1	...	...	...	1
WD 1550+130	PG 1550+131	DA+dM	3	...	2	...	6
WD 1559+369	G180−023	DAV	2	...	1	...	4
WD 1615−154	EG 118	DA1.7	2	1	1	...	4
WD 1620−391	CD −38 10980	DA2	13	1	10	...	159
WD 1631+781	WD 1631+781	DA1+dM	1	1	1	...	3
WD 1634−573	HD 149499B	DOZ1+K0 V	3	...	3	...	6
WD 1636+351	KUV 433−03	DA1.5	4	...	1	...	5
WD 1639+537	GD 356	DCP7	1	1	1	...	4
WD 1645+325	GD 358	DBZV2	6	4	5	...	17
WD 1647+591	G226−29	DAV4.7	5	...	3	...	8
WD 1650+724	HS 1650+7229	DA1	1	...	...	...	1
WD 1654+160	PG 1654+160	DBV	2	...	1	...	3
WD 1657+343	PG 1657+344	DA1	1	...	...	...	1
WD 1658+440	PG 1658+441	DAP2d	2	...	1	...	4
WD 1707+427	PG 1707+427	DOZ.5	1	...	1	...	2
WD 1708−147	L845−70	DQ5	1	...	...	...	1
WD 1708−871	JL 1	DB	1	...	...	...	1
WD 1709+230	GD 205	DB4	1	1	...	...	2
WD 1713+695	G240−51	DA3	1	...	1	...	2
WD 1725+586	PG 1725+587	DA1	2	...	...	...	2
WD 1734+742	HD 160538	DA1.5+K0 IV	3	2	2	...	7
WD 1735−318	NGC 6405−1	DA.5	2	1	...	...	3
WD 1736+133	HD 160365B	DA2+F6 III	2	...	1	1	4
WD 1738+669	RE J1738+665	DA1	1	...	...	...	2
WD 1743−521	BPM 25114	DAP6	1	...	1	...	2
WD 1749+717	HS 1749+7145	DAO.5	1	...	...	...	1
WD 1800+685	KUV 18004+6836	DA1	1	1	...	...	2
WD 1803−482	HD 165141	DA+G8 III	1	...	...	...	1
WD 1819+580	RE J1820+580	DA1	1	1	...	...	2
WD 1821+643	K1−16	DOZ.4	7	2	3	...	31
WD 1822+410	GD 378	DBAZ4	1	...	1	...	2
WD 1827+778	HS 1827+7753	DA.5	1	...	...	...	1
WD 1828+668	KUV 18284+6650	DA	1	...	...	...	1

TABLE 2—*Continued*

WD Number	Alt. ID	Spectral Type	SWP		LWP/LWR		Total
			LAP	SAP	LAP	SAP	
WD 1830+721	HS 1830+7209	DO.6	1	...	...	...	1
WD 1837−619	BPM 11668	DC5	1	...	1	...	2
WD 1845+683	KUV 18453+6819	DA1.5+dM	1	...	...	...	1
WD 1845+019	Lanning 18	DA1.5	1	1	...	...	2
WD 1855+338	G207−009	DAV	1	...	1	...	2
WD 1900+705	GW+70 8247	DAP4.5	5	...	4	...	8
WD 1917−077	LDS 678A	DBQA5+dM6	5	...	4	...	11
WD 1919+145	GD 219	DA3.5	1	...	1	...	2
WD 1921−566	RE J1925−566	DA1+G5 V	1	...	...	...	1
WD 1935+276	G185−032	DAV4	2	...	1	...	3
WD 1936+327	EG 226	DA2.5	1	...	...	...	1
WD 1940+374	L1573−031	DB3.2	1	...	1	...	2
WD 1950−432	MCT 1950−432	DA1	2	...	1	...	3
WD 1953−011	L997−21	DA6.4	1	...	1	...	3
WD 2000−561	MCT 2000−5611AB	DA	1	...	1	...	2
WD 2004−605	RE J2009−605	DA1	1	...	...	...	1
WD 2007−303	LTT 7987	DA4	1	...	1	...	2
WD 2010+310	GD 229	DBP3.1	3	...	9	...	19
WD 2011+398	RE J2013+400	DAO+dM4e	2	...	1	...	4
WD 2014−575	L210−114	DA2	3	...	2	...	5
WD 2020−425	MCT 2020−4234	DA1.7	1	...	...	...	1
WD 2028+390	GD 391	DA2	3	1	2	...	6
WD 2032+248	Wolf 1346	DA2.5	2	1	2	...	5
WD 2034−532	BPM 26944	DB4	1	...	...	...	1
WD 2039−202	L711−10	DA2.5	2	...	1	...	3
WD 2046+396	KPD 2046+3940	DA.8	1	2	1	...	4
WD 2047+372	G210−036	DA4	2	...	1	...	3
WD 2059+316	G187−15	DQ5	1	...	...	...	1
WD 2105−820	BPM 1266	DA5	1	...	1	...	2
WD 2110+300	HD 202109	DA4	4	...	2	1	7
WD 2111+498	GD 394	DA1.5	4	1	7	...	13
WD 2115+339	RX J 2117+3417	PG 1159	3	...	...	...	3
WD 2116+736	KUV 21168+7338	DA1	1	1	...	...	2
WD 2117+539	G231−040	DA3.5	2	...	1	...	3
WD 2123−226	HD 204075	DA2+G4 Ib	2	...	1	...	3
WD 2124+191	HD 204188	DA1.5+A8 V	10	...	1	...	12
WD 2126+734	GW+73 8031	DA4	1	...	1	...	2
WD 2129+000	LDS 749B	DB3.5	4	...	4	...	8
WD 2136+828	G261−045	DA3	1	...	1	...	2
WD 2140+207	G126−27	DQ5.7	1	...	...	...	1
WD 2146−433	MCT 2146−4320	DA.74	1	...	...	...	2
WD 2147+280	G188−027	DB4.5	1	...	...	...	1
WD 2149+021	G93−048	DA3	3	...	3	...	6
WD 2152−548	RE J2156−543	DA1	1	1	...	...	2
WD 2153−419	MCT 2153−4156	DA1	1	...	1	...	2
WD 2159−414	MCT 2159−4129	DA.89	1	...	1	...	2
WD 2205+250	RE J2207+25	DA2	1	...	...	...	1
WD 2207−303	RE J2210−300	DA2	2	...	...	...	2
WD 2211−495	RE J2214−491	DA.76	6	8	6	...	21
WD 2216−657	L119−34	DZ5	1	...	1	...	2
WD 2224−344	LDS 785A	DB3	1	...	1	...	2
WD 2237+819	HS 2237+8154	DA+dM	1	...	...	...	1
WD 2246+066	HS 2246+0640	DA.51	1	...	1	...	2
WD 2246+223	G67−023	DA4.9	2	...	...	...	2
WD 2257−073	HD 217411B	DA1.5+G5 V	1	...	...	...	1
WD 2304+251	HD 218356	DA1+G0 V	5	...	1	...	7
WD 2309+105	GD 246	DA1	8	2	4	...	14
WD 2316+123	KUV 813−14	DAO4	2	...	2	...	4
WD 2316−173	L791−40	DBQA5	2	...	2	...	4
WD 2321−549	RE J2324−544	DA1	1	...	...	...	1
WD 2324+397	HS 2324+3944	DO.4	1	...	...	...	1
WD 2326+049	G29−38	DA4.5	3	1	5	...	10
WD 2331−475	RE J2331−471	DA1	5	1	1	...	7
WD 2333−002	PG 2333−002	DA??	2	...	...	...	2

TABLE 2—*Continued*

WD Number	Alt. ID	Spectral Type	SWP		LWP/LWR		Total
			LAP	SAP	LAP	SAP	
WD 2341+322	L1512−034B	DA3	1	...	1	...	2
WD 2349+286	PG 2349+286	DA1	1	...	1	...	2
WD 2350−706	HD 223816B	DA1+G0 V	1	...	1	...	2
WD 2353+026	PG 2353+026	DA1	3	...	2	...	6
WD 2357+296	PG 2357+297	DA1	3	1	1	...	5
WD 2359−434	L362−081	DA5	1	...	...	...	1
SD 0216+032	PG 0216+032	sdOC	1	...	1	...	2
SD 0906+597	PG 0906+597	sdB	1	...	...	...	1
SD 0901+314	CBS 2	sdO	1	...	...	...	1
SD 1124−620	CS 1244−62	???	1	...	1	...	2
SD 1148−230	EC 1148−2	sdB	1	...	...	...	1
SD 1302+283	PG 1302+283	sdB	1	...	1	...	2
SD 1348+369	PG 1348+369	sdB	1	...	1	...	2
SD 1520+205	PG 1516+025	sdO	6	...	1	...	10
SD 1543+454	PG 1543+454	sdO	1	...	...	...	1
MS 0448+109	HD 30810	G8 III	1	1	...	...	2
MS 0449+136	HD 30869	F5	1	1	...	...	2

contamination (Caplinger 1995) began to be noticed in the LWP camera in 1993 when the telescope was pointed at high beta angles (near the Sun). The "LWP streak" manifested itself as a solar continuum flooding the image that produced a solar type spectrum longward of about 1600 Å. Examples of spectra containing this contamination include WD 0406+169 (LB 227). Since there were a number of LWP spectra of LB 227 with and without the effect, we produced two versions of the final co-added spectrum for this star, one free from contamination and one including the effect. Other examples include WD 1520+525 (PG 1520+525) and WD 2011+398 (RE J2013+400), where the contamination was left in place because there were no long-wavelength spectra free from the effect. The log files of the affected stars contain notes regarding the contamination.

Mismatched short- and long-wavelength spectra.—Several stars show strong differences in flux level between the SWP and LWP/LWR flux levels at 1900 Å. Examples include WD 0000−170 (LTT 11) and WD 1654+160 (PG 1654+160). In situations where this was observed to occur notes have been placed in the log files.

Inconsistent flux levels.—In several cases there was clear inconsistency between the flux levels in the spectra being co-added. For example, in the case of WD 0302+027 (Feige 31) five spectra (four SWP LAP and one LWP LAP) were compared. One of the SWP spectra contained no flux, while the other three differed in flux by 25%–63%. However, one spectrum, SWP 22289, was found to agree with LWP 02797 in the region of overlap so the other two SWP spectra were corrected to SWP 22289 and co-added. No explanation of this discrepancy was evident in the spectral headers.

Null-spectra.—Several stars show no detectable flux in either camera. In general, for completeness, we retained these in the archive. Possible explanation include the star being too faint, too cool, or simply not in the spectrograph aperture. Examples include WD 0046+051 (van Mannen 2) and WD 0216+143 (PG 0216+143).

Non–white dwarfs.—Several stars were classified as white dwarfs but are actually sdB or sdO subdwarfs. Examples include PG 0906+597, CBS 2, CS 1244−62, EC 1148−2, PG 1302+283, PG 1348+369, PG 1516+020, and PG 1543+454. We have retained these stars in the archive with "SD" rather than "WD" identification. The main-sequence stars HD 30810 and HD 30869 were observed by Böhm-Vitense (1995) in an attempt to spectroscopically identify white dwarf companions to F stars in the Hyades cluster. In neither case was a white dwarf unambiguously discerned.

4. CONTENTS OF THE DATA ARCHIVE

4.1. *IUE Observations of White Dwarfs*

In low-dispersion mode, *IUE* possessed sufficient sensitivity to observe a variety of degenerate stars ranging in brightness from visual magnitude 8 down to nearly magnitude 18, and in temperature from the very hottest stars with effective temperatures in excess of 100,000 K to those near $T_{\rm eff} = 5000$ K. This range resulted in a significant expansion in the types of white dwarf phenomena that could be studied at UV wavelengths. For example, an understanding of the importance of opacity from the H_2^+ quasi-molecule was first recognized in *IUE* spectra of cool DA stars (Koester et al. 1985 and Nelan & Wegner 1985) . Additionally, the spectra of a number of hot white dwarfs in binary systems containing luminous main-sequence stars were studied for the first time using *IUE* (Barstow et al. 1994 and Vennes, Christian, & Thorstensen 1998).

White dwarfs are conveniently classified in terms of their spectral types. The present classification scheme was introduced by Sion et al. (1983) and has been further refined in MS99. The archive of white dwarfs observed with *IUE* contains examples of many of these spectral types. White dwarfs observed with *IUE* naturally fall into several general categories based on their spectral type or binary status. These classes are the H-rich or DA white dwarfs, the He-rich or DB and DO white dwarfs, including the PG 1159–like stars, miscellaneous spectral types such as magnetic white dwarfs and carbon-rich white dwarfs, and binary systems containing hot white dwarfs. In this section we discuss these categories and illustrate examples of each from the archive.

4.2. H-*Rich White Dwarfs*

White dwarfs having predominantly H-rich photospheres constitute the vast majority (up to 80%) of all known white dwarf stars. They are classified as DA if they exhibit only hydrogen Balmer lines in the optical, and DAO or DAB (see § 4.3) if they also contain, respectively, weak He II or He I lines in the optical. Many hot DA stars, such as G191-B2B, also possess narrow interstellar-like lines due to heavy elements. In general such heavy element lines are not resolved with *IUE* at low dispersion but are frequently apparent in *IUE* echelle spectra (see HBS). In Figure 5 we show examples of the *IUE* spectra of six hot DA white dwarfs ordered as a function of effective temperature. At low dispersion the only stellar feature present in these spectra is the broad H I Lyα line that can be seen to strengthen with diminishing $T_{\rm eff}$.

Low-dispersion *IUE* observations of hot DA white dwarfs have focused primarily on the use of the H I Lyα profiles and UV stellar energy distributions to estimate effective temperatures and surface gravities. Holberg, Wesemael, & Basile (1986) analyzed the Lyα profiles of 12 hot DA stars to determine the $T_{\rm eff}$ and log g over the temperature range 20,000–60,000 K. Although such estimates are generally in good agreement with optical determinations based on the detailed fitting of Balmer profiles, often external constraints such as optical magnitudes or trigonometric parallaxes are required to resolve the strong correlations of $T_{\rm eff}$ and log g resulting from the Lyα profile fits. Finley, Basri, & Bowyer (1990) used ratios between *IUE* and optical fluxes to

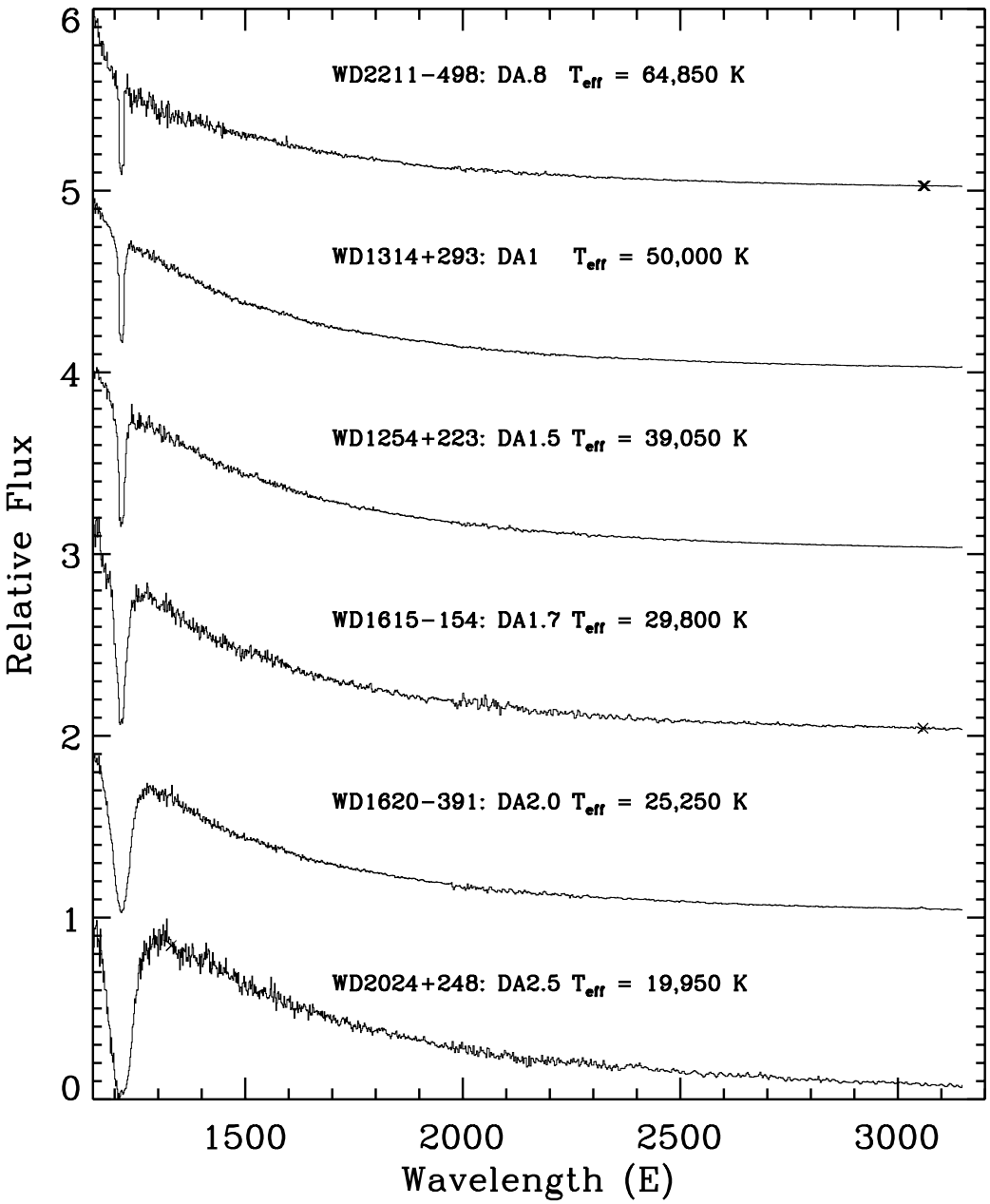

FIG. 5.—Sequence of six hot DA white dwarfs covering temperature range 65,000–20,000 K and showing the increase in strength of the stellar Lyα line as a function of decreasing temperature. Spectra have been normalized and offset vertically by 1.0.

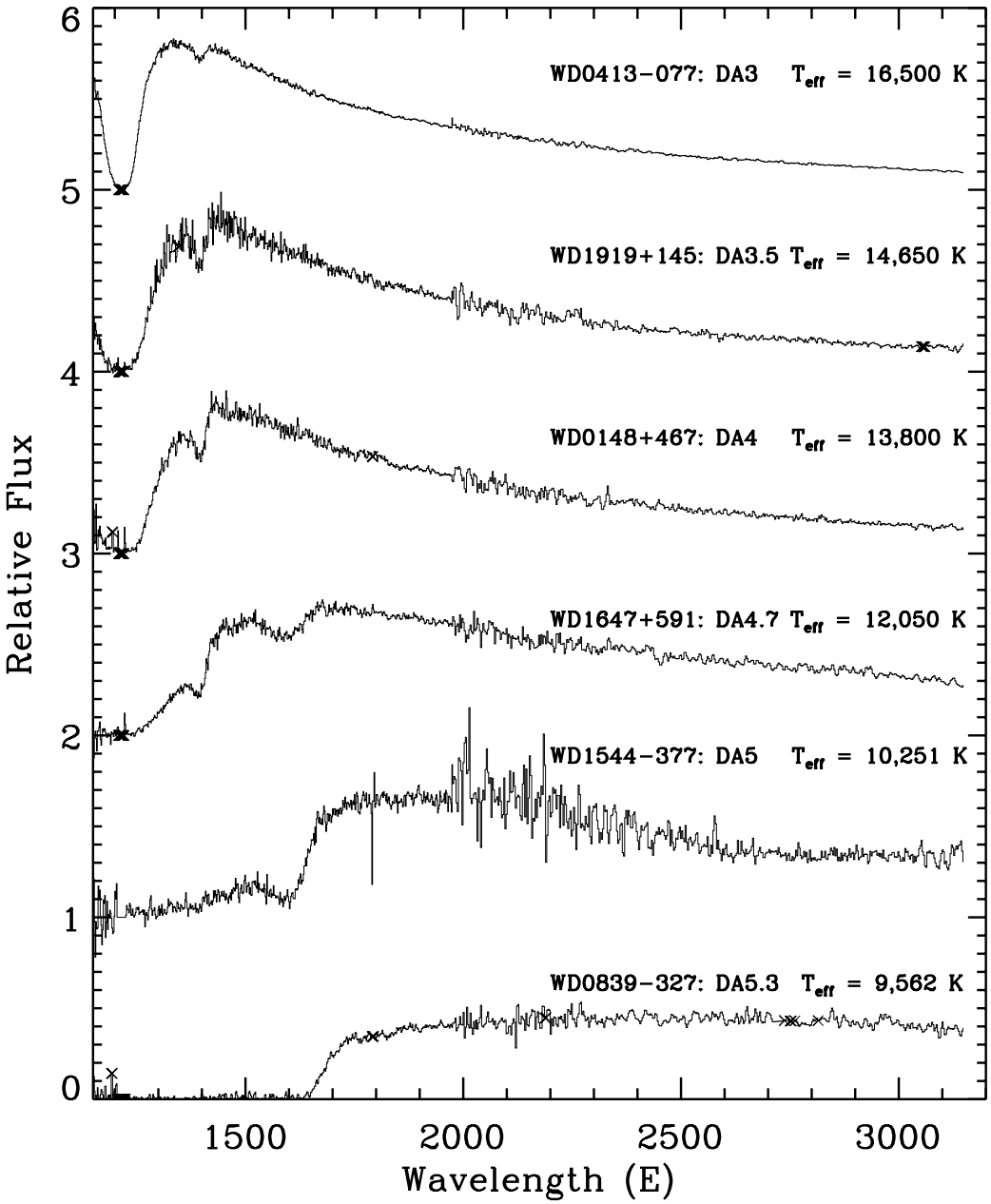

FIG. 6.—Sequence of six cool DA white dwarfs covering the temperature range 16,500–9500 K showing the development of the H_2^+ satellite features at 1400 and 1600 Å as a function of decreasing temperature. Spectra have been normalized and offset vertically by 1.0.

estimate temperatures for a number of DA stars having temperatures above 25,000 K. Both Holberg et al. (1986) and Finley et al. (1990) noted the presence of wavelength dependent residuals in the early *IUE* absolute flux calibration. This eventually led to the adoption of DA white dwarfs as flux standards for the NEWSIPS data (see NL96) and for other UV space missions.

At effective temperatures below approximately 20,000 K, broad satellite features of the H I Lyα line begin to be apparent at wavelengths of 1400 and 1600 Å. These features are due to transitions in the quasi-molecule, H_2^+, and were first observed in the DA white dwarf 40 Eri B by Greensetein & Oke (1979). The satellite Lyα features were subsequently explained theoretically by Koester et al. (1985) and Nelan & Wegner (1985). In Figure 6 we show a sequence of six cooler DA stars that exhibit these features. Discussions of these H I satellite features in *IUE* spectra is contained in Koester & Allard (1993) and Koester & Holberg (2001).

4.3. He-*Rich White Dwarfs*

White dwarfs that show He II or He I photospheric lines but no H I in the optical are classified as, respectively, DO or DB. The DO classification extends from very high effective temperatures, in excess of 100,000 K, to as low as 40,000 K. The hottest and most luminous of these objects are the PG 1159 stars that are believed to be descended from the O VI central stars. At low dispersion, *IUE* spectra of DO stars show the He II Balmer α line at λ1640 and the He II Balmer β line at λ1216; heavy interstellar H I absorption often

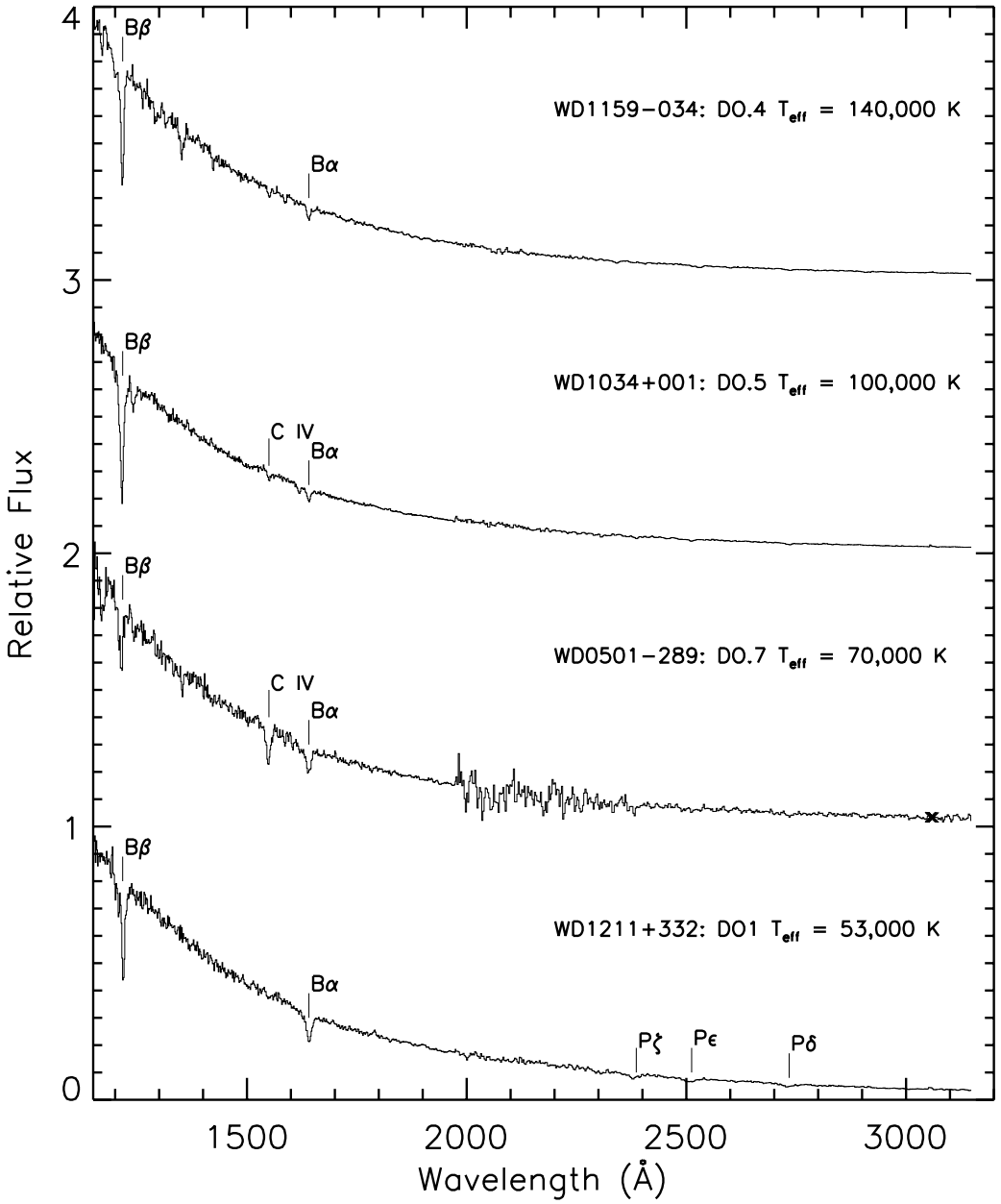

FIG. 7.—Sequence of four hot DO white dwarfs covering temperature range 140,000–53,000 K. The most prominent spectra features seen in the DO stars are the He II Balmer α and β features. In cooler stars such as WD 1211+332 (HZ 21) lines due to the He II Paschen series can be seen. In a few DO stars such as WD 0501−289 strong features due to CIV and other elements can be seen in low-dispersion spectra. Spectra have been normalized and offset vertically by 1.0.

contaminates the latter. In several stars, lines due to the He II Paschen series can also been seen at wavelengths longward of 2000 Å. In a few high-quality spectra, even features due to heavy elements such as C IV are even evident at low dispersion. A temperature sequence of DO stars observed with *IUE* is shown in Figure 7.

The DB white dwarfs show He I lines in the optical, and some, including WD 1645+325 (GD 358), exhibit C I lines at echelle resolution in the UV (Provencal et al. 1996, and Sion et al. (1989) In addition to the DB Gap, there also exists a zone of pulsational instability, the V777 Her stars. *IUE* observations have been instrumental in trying to determine the blue and red ends of this gap (Beauchamp et al. 1999). In Figure 8 we show a temperature sequence of DB stars observed with *IUE*.

4.4. *The Hybrid* H-He *Stars*

A small fraction of white dwarfs below $T_{\rm eff} \sim 30,000$ K show hybrid H I and He I spectra, these are the DAB and DBA white dwarfs. Interest in these stars arises from the hope that they may provide a key to understanding the chemical evolution of white dwarf atmospheres, in particular the DB gap. The DB gap refers to the apparent absence of the He-rich stars in the temperature range of 45,000–30,000 K. (Liebert et al. 1986), which implies that white dwarf photospheres undergo compositional changes as they cool. Several explanations have been suggested for the existence of the DB gap, including the onset of convection and a subsequent mixing of He and H layers as stars reach the cool edge of the DB gap. The

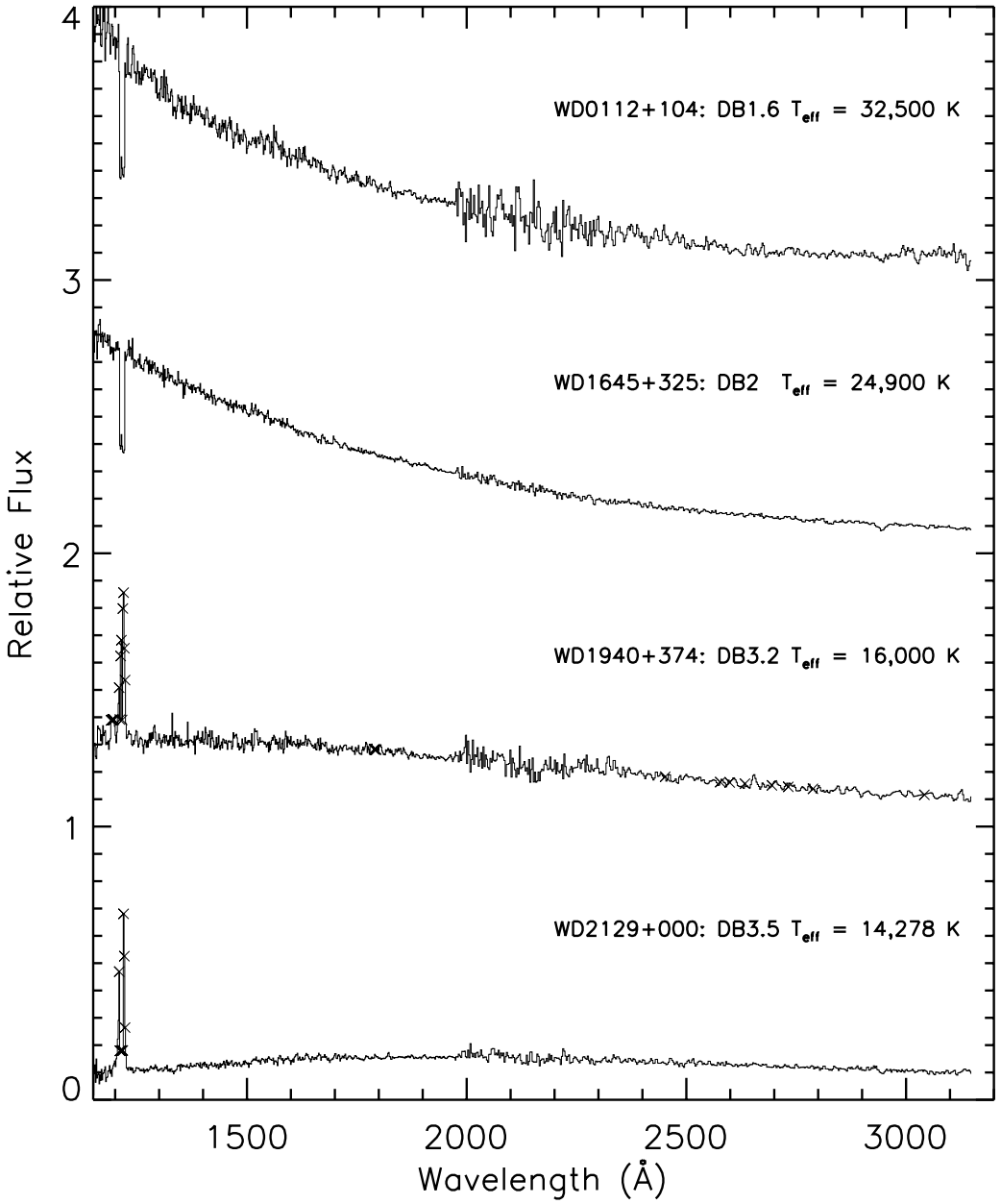

FIG. 8.—Sequence of four DB white dwarfs covering temperature range 31,500–15,500 K. Spectra have been normalized and offset vertically by 1.0.

possibility that DAB stars may represent a brief transitional phase in this process remains intriguing. Alternately, some hybrid DAB and DBA stars could simply represent the composite spectrum of a double degenerate binary system containing DA and DB. Indeed, for the DAB star WD 0453−295, Wesemael et al. (1994) have been able to fit its spectrum and energy distribution with a combination of a 16,000 K DA and a 13,000 K DB white dwarf. Attempts to fit other stars, such as the DAB white dwarf WD 1302+597 (GD 323), using various models including composite spectra or with models having stratified compositions have not been generally successful (Koester, Liebert, & Saffer 1994). In spite of such difficulties *IUE* observations have proved especially valuable in determining the effective temperatures of these stars. In Figure 9 we show a *IUE* spectra of four hybrid stars.

4.5. *Miscellaneous Spectral Types*

In addition to the H-rich and He-rich white dwarfs, there also exist a number of other spectral classifications which indicate the presence of features due to atomic carbon (the DQ white dwarfs), strong magnetic fields (the DP and DH stars), and cooler stars with metal lines from species such as Mg, Ca, and Fe (the DZ white dwarfs). Although these classes represent a distinct minority of all white dwarfs, they may provide useful clues as to the evolution of white dwarfs, nature of their progenitors as well as a history of their interactions with the interstellar medium.

In Figure 10 we show a sequence *IUE* archive spectra of four DQ white dwarfs, WD 1917−077 (LDS 678A), WD 0115+159 (G33−49), WD 1142−645 (LP 145−141), and WD 0426+588 (Stein 2051 B). Our values of $T_{\rm eff}$ are taken from Weidemann & Koester (1995), except for

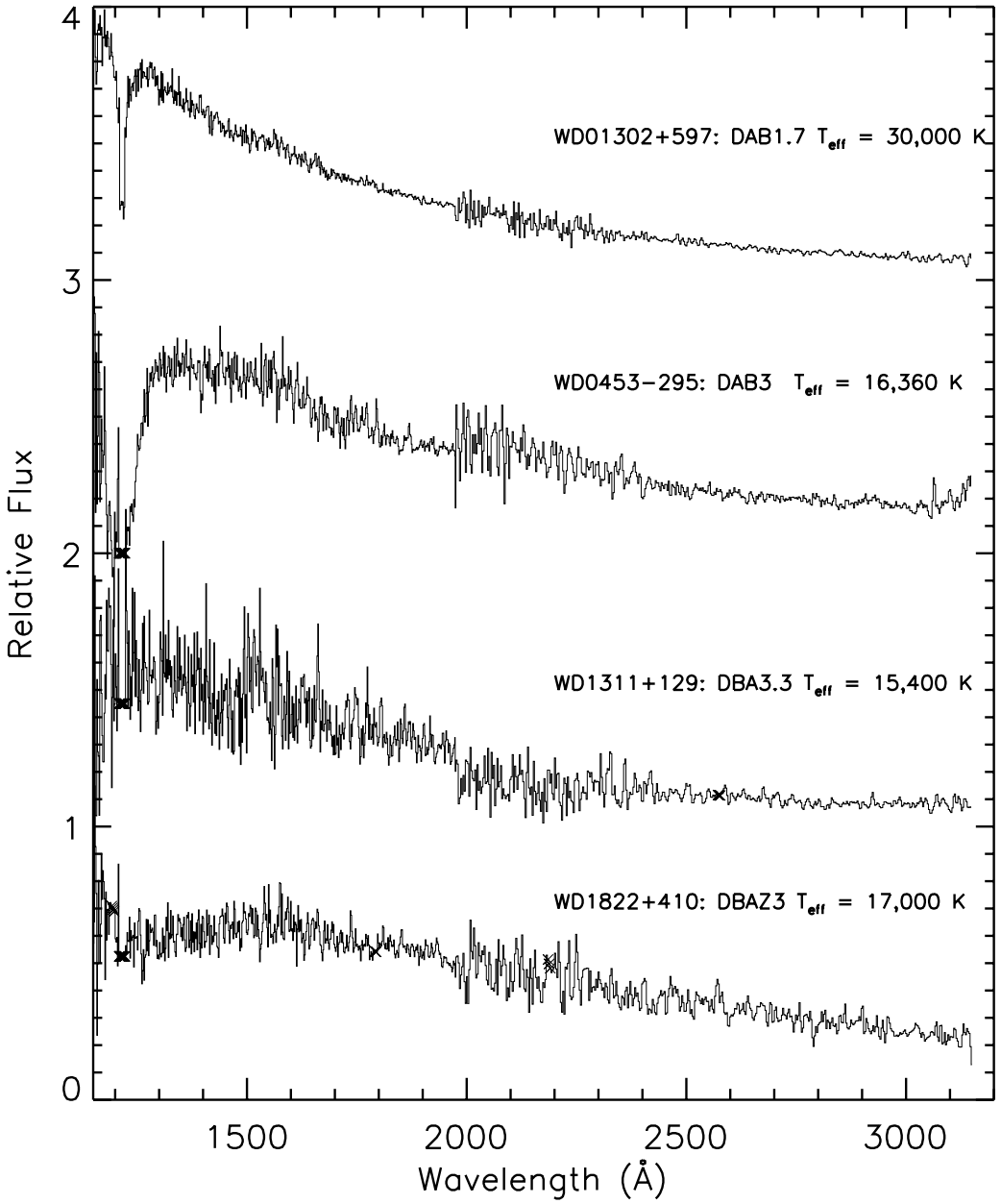

FIG. 9.—Sequence of four DAB and DBA white dwarf spectra. Spectra have been normalized and offset vertically by 1.0.

WD 0426+588 in which the reference is to Wegner (1983) and WD 1917−077 which is taken from Oswalt et al. (1991). It is interesting to note that the C I λ2479 line which Oswalt et al. observed with *IUE* at high dispersion to determine the gravitational redshift of WD 1917−077 is strong enough to be seen at low dispersion. The DQ stars have He-rich photospheres but in general are too cool to show significant He I lines; however, they do show C I features in the optical and UV. *IUE* observations of the DQ stars have been important in establishing both the effective temperatures and the C/He abundance in the photospheres in these stars. The presence of carbon is believed due to a process of convective dredge-up of C which mixes into the outer He layers.

The two upper spectra in Figure 11 are of the strongly magnetic DP stars, WD 0316−849 (RE J0317−853) and WD 2010+310 (GD 229), where our values of $T_{\rm eff}$ are taken from, respectively, Burleigh, Jordan, & Schweizer (1999) and Wickramasinghe & Ferrario (2000). Only about 5% of the cataloged white dwarfs have observable magnetic fields, although selection effects act to may conceal a true fraction which could be higher (see Liebert, Bergeron, & Holberg 2002). Nonetheless, very few stars are known to have magnetic fields as high as those in PG 1031+234 (500–1000 MG) and RE J0317−853 (200–800 MG). PG 1031+234 was first observed with *IUE* by Schmidt et al. (1986), who identified the strong feature seen at 1335 Å as the σ^+ Zeeman component of H I Lyα. Schmidt et al. also employed the *IUE* and optical energy distributions to help estimate $T_{\rm eff} = 15,000$ K for this star. RE J0317−853 is a rapidly rotating ($P_{\rm rot} = 725$ s), massive ($M \sim 1.35\ M_{\odot}$), magnetic white dwarf. The extreme nature of this *ROSAT* source was first revealed by optical follow-up observations by Barstow et al. (1995), who used *IUE* to initially estimate a temperature near 50,000 K. The *IUE* spectrum of RE J0317−853

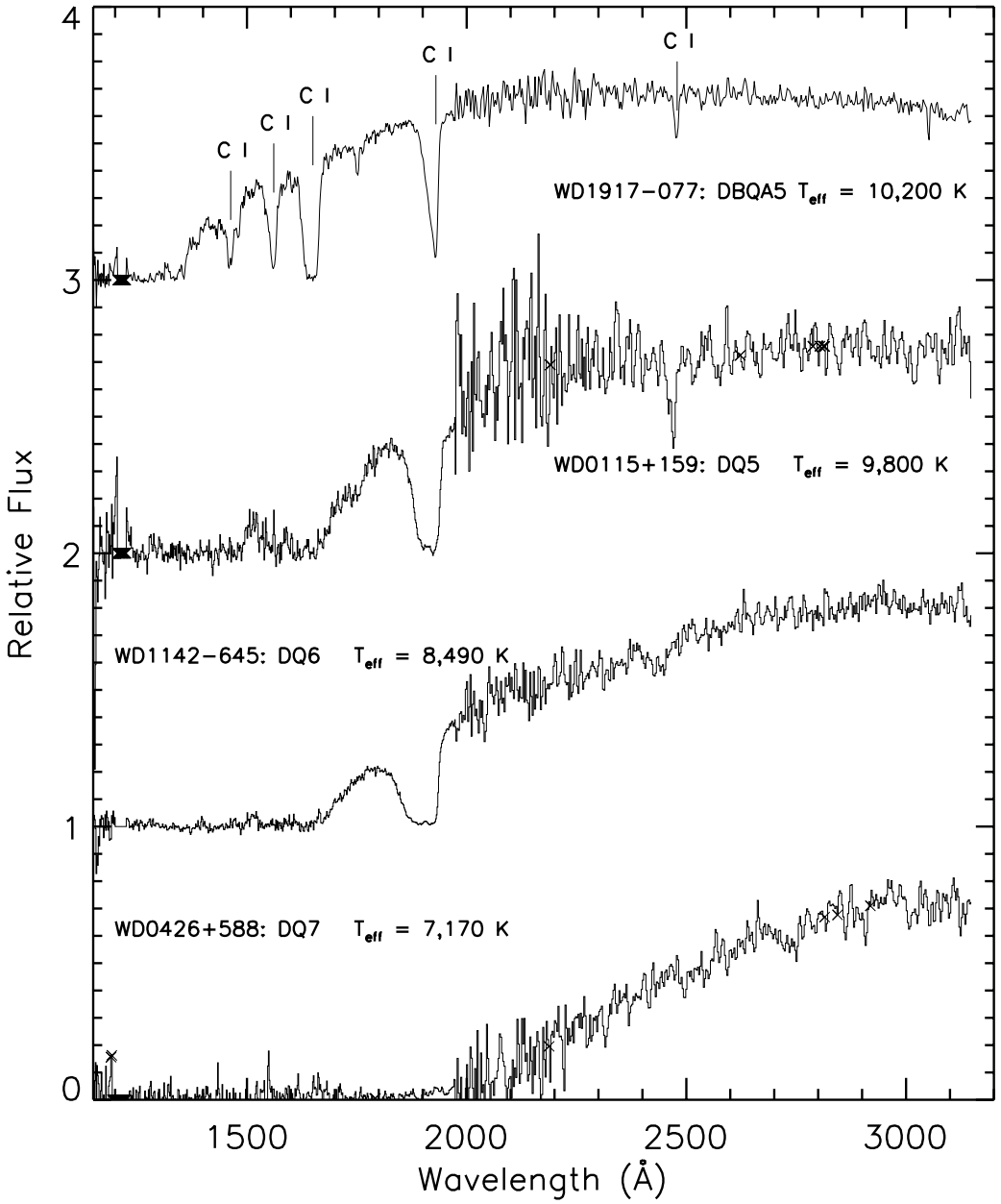

FIG. 10.—Sequence of four DQ white dwarf spectra. The locations of the pressure broadened C I lines are indicated in the top plot. Spectra have been normalized and offset vertically by 1.0.

reveals the complexity of its global magnetic field. The two broad features located at 1300 and 1340 Å in Figure 11 correspond to redward Zeeman shifted Lyα lines for respective polar field strengths of <220 MG and >450 MG. Because the *IUE* spectra were exposed over many rotation periods these features record the two dominant field strengths which are separated by approximately one half-cycle in rotation phase. The broad feature at 1195 Å is the blueward Zeeman shifted component of Lyα for the "low" (<220 MG) field phase. When the "high" (>450 MG) fields dominate, this feature is shifted out of the *IUE* wavelength range. Time-resolved spectra *HST* FOS spectra of RE J0317−853 obtained by Burleigh et al. (1999) can be best modeled with a complex field described by low-order Legendre polynomial expansions. Burleigh et al. refine the temperature of RE J0317−853 to be nearer 40,000 K. Another notable magnetic white dwarf is WD 1639+357 (GD 356), which shows Zeeman splitting of emission lines at Hα and Hβ. The ultraviolet spectrum of this star, however, reveals no emission at Lyα, only a continuum energy distribution (Shipman 1986).

The two lower spectra in Figure 11 are of the DZ stars, WD 1225−079 (K789−37) and WD 2216−657 (L119−34), where our values of $T_{\rm eff}$ are taken from Wolff, Koester, & Liebert (2002). The DZ stars are cool He-rich white dwarfs that exhibit features in the optical and UV due to heavy elements such as Mg, Ca, and Fe. The presence of these metals in cool stars, long after they should have diffused out of the stellar photosphere, is believed to be due to accretion of interstellar material, mostly in the from of dust grains, during episodic encounters of these stars with dense interstellar clouds (see Dupuis et al. 1992, 1993a, 1993b). However,

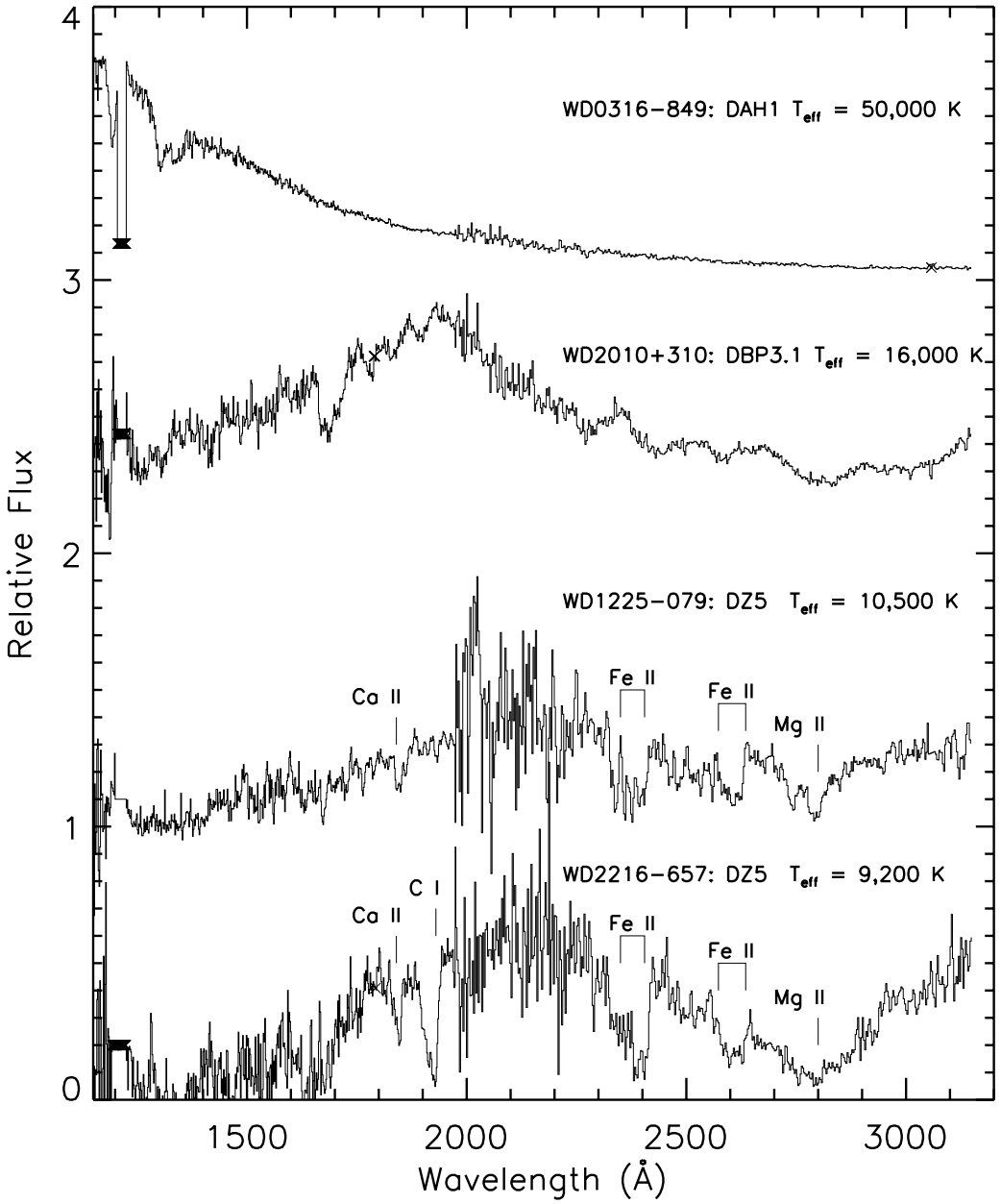

FIG. 11.—*Top two spectra*: Two strongly magnetic white dwarfs. *Bottom two spectra*: Two DZ white dwarfs showing strong features due to C I, Mg II, Ca II, and Fe II. Spectra have been normalized and offset vertically by 1.0.

Koester et al. (2003) and others have noted the frequency of DZ stars is too high to be explained by interstellar accretion, and alternative explanations need to be considered. *IUE* observations have greatly extended our study of these stars by providing access to the UV, where many strong features such as Mg I λ2852, Mg II $\lambda\lambda$2796, 2803, and Ca II λ1840 can be observed. Additionally, UV continuum observations are important for achieving accurate estimates of the effective temperature and determinations of the photospheric H/He ratios (see Wolff et al. 2002).

4.6. *Binary Systems*

One of the major achievements of *IUE* was the ability to observe the UV spectra of white dwarfs in binary systems dominated by luminous main-sequence stars. Often called Sirius-like systems, these binaries include main-sequence stars of spectral type late K or earlier whose optical luminosity effectively obscures the white dwarf. As in the case of Sirius B, direct observations can be extremely difficult or even impossible. In the UV, however, the rising short-wavelength energy distribution of a hot white dwarf can come to actually dominate that of more luminous main-sequence companions as early as A4 V. The study of these systems is important in several respects. First, identification of such systems can shed light on the true number of nearby white dwarfs that reside in such systems. Second, the white dwarf progenitor was originally the more massive component of the system and the evolutionary timescale for the system can be gauged from the cooling age of the white dwarf. These systems can also provide useful estimates of the white dwarf initial-to-final mass relation. Finally, the white dwarfs in short period, Sirius-like, systems can be studied as

either single or double line spectroscopic binaries or in rare cases as astrometric binaries, from which useful dynamic mass estimates for the white dwarf can be obtained.

Prior to *IUE*, the number of known Sirius-like systems was relatively small since the white dwarf had either been accidently discovered as in the case of HD 149499 B or was suspected from astrometric or radial velocity studies. *IUE* observations of late type stars led to the serendipitous discovery of several Sirius-like systems (see Fekel & Simon 1985; Böhm-Vitense 1992, 1993). Additionally, Landsman, Simon, & Bergeron (1996) observed two F stars that exhibited UV excesses in the *TD-1* UV sky survey. The *IUE* spectra of these stars clearly revealed white dwarfs and yielded useful estimates of $T_{\rm eff}$ and log g. The importance of *IUE* observations for the study of such systems became even more apparent in the early 1990s when the all-sky EUV surveys conducted by *ROSAT* and the *Extreme Ultraviolet Explorer* (*EUVE*) found a host of Sirius-like systems. These surveys identified more than two dozen such systems from the presence of a strong EUV continuum that could not be readily explained in terms of coronal activity from the primary star (see Barstow et al. 1994 and Vennes, Christian, & Thorstensen 1998). *IUE* observations were often critical, first in confirming the presence of the white dwarfs, and second in estimating the temperature and gravity of the white dwarf. The *IUE* archives contain over 30 such systems. In Figure 12 we show the composite spectra of several of these systems.

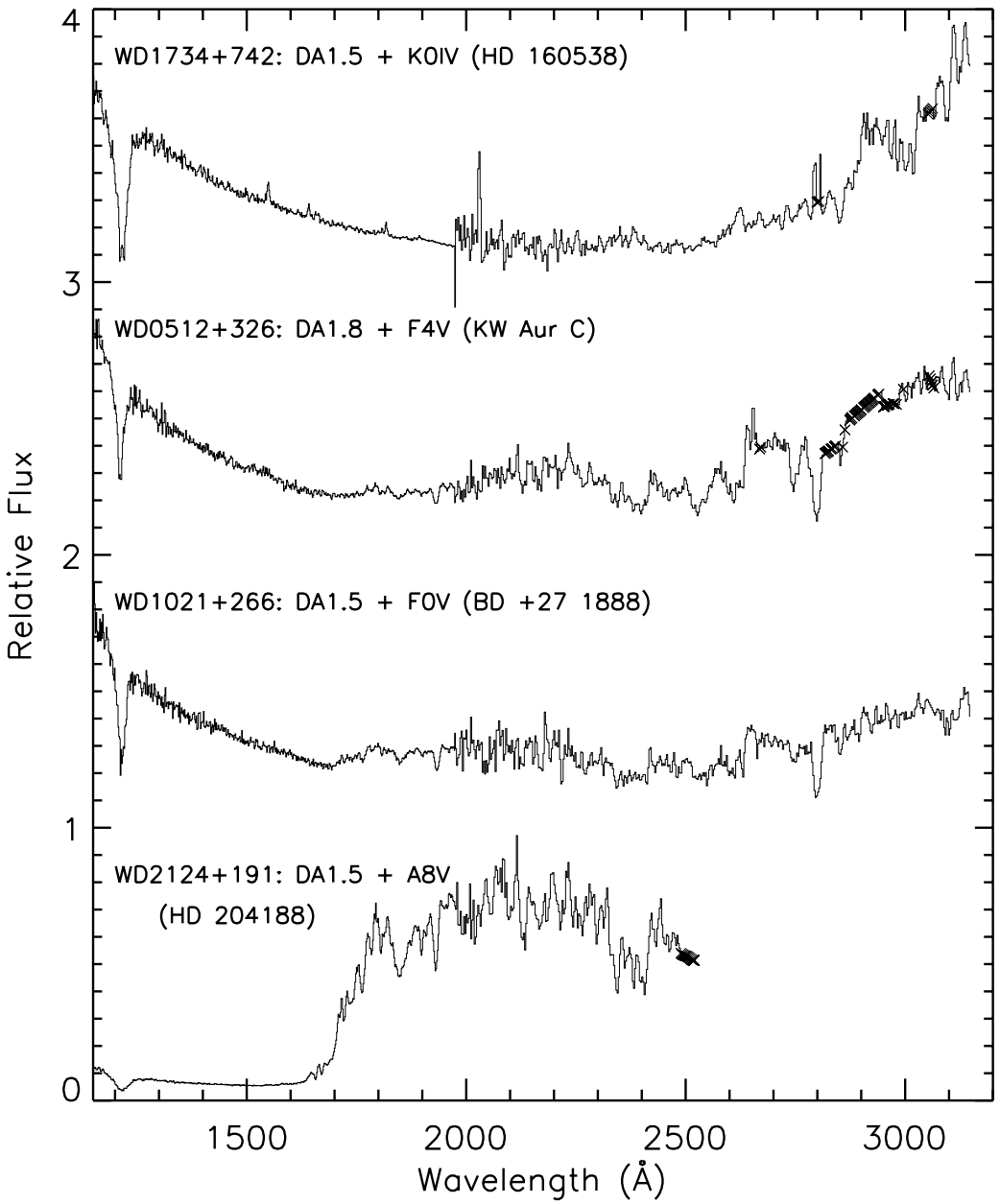

FIG. 12.—Sequence of four composite spectra of binary systems consisting of hot DA white dwarf and main-sequence primary stars of varying spectral type from KO IV to A8 V. This illustrates how the balance of flux shifts with wavelength as the spectral type of the primary changes. Spectra have been normalized and offset vertically by 1.0.

Another class of binary systems where effective temperatures derived from *IUE* low dispersion have proved of great use are the Pre-Cataclysmic variable systems, in which a cool M dwarf is in a short period orbit about a hot white dwarf. Examples of such systems include V471 Tau and Feige 24 among others. Although the white dwarfs can be detected spectroscopically in the optical, the contamination of the H I Balmer lines by the cool companion, principally by the emission lines from the reflection effect, inhibits the detailed study of the white dwarf. *IUE* observations have proved invaluable in determining the effective temperature and gravity of the white dwarf in these systems.

Barium stars are red giants exhibiting anomalously high abundances of heavy elements, in particular barium. Suspicion that such chemical enrichments were the result of binary star evolution arose from the observation that most of these stars exhibited radial velocity variations due to unseen subluminous companions. Böhm-Vitense (1980) used *IUE* to detect the UV continuum of the white dwarf WD 2123−226 in the spectrum of ζ Cap. This was followed by several other detections, including WD 2111+498 in ζ Cyg (Dominy & Lambert 1983). It is hypothesized that the binary components in most barium stars are white dwarfs which have transferred *s*-processed material to the present luminous companion through mass loss during its asymptotic giant phase.

We wish to thank Derek Massa for generously providing an advance copy of the MF00 corrections. We are also grateful to Jim Collins for help with writing our IDL reduction procedures, to Bob Lurgio for the summer he devoted to processing the spectra, and to Kate Magargal for assistance with validation of the tables. We wish to acknowledge support from NASA grant NAGW5-9182. M. A. B. and M. R. B. were supported by the Particle and Astronomy Research Council, UK. All of the data presented in this paper were obtained from the Multimission Archive at the Space Telescope Science Institute (MAST). STScI is operated by the Association of Universities for Research in Astronomy, Inc., under NASA contract NAS5-26555. Support for MAST for non-*HST* data is provided by the NASA Office of Space Science via grant NAG5-7584 and by other grants and contracts. The contents of this archive are available in several formats. The identification of the final spectra is by WD number. Spectra can be viewed with the White Dwarf Database.[1] Data for all spectra used in the archive can be obtained in both FITS format and as formatted text files,[2] access is also available to individual MF00 corrected spectra upon request. Users are advised to consult the log files for all spectra.

[1] See http://procyon.lpl.arizona.edu/WD.
[2] See http://vega.lpl.arizona.edu/newsips/low/.

REFERENCES

Barstow, M. A., Holberg, J. B., Cruise, A. M., & Penny, A. J. 1997, MNRAS, 290, 505
Barstow, M. A., Holberg, J. B., Fleming, T. A., Marsh, M. C., Koester, D., & Wonnacott, D. 1994, MNRAS, 270, 499
Barstow, M. A., Jordan, S., O'Donoghue, D., Burleigh, M. R., Napiowotzki, R., & Harrop-Allin, M. K. 1995, MNRAS, 277, 971
Beauchamp, A., Wesmael, F., Bergeron, P., Fontaine, G., Saffer, R. A., Liebert, J., & Brassard, P. 1999, ApJ, 516, 887
Bica, E., Bonatto, C., & Giovannini, O. 1996, A&AS, 119, 211
Bohlin, R. C. 1996, AJ, 111, 1743
Bohlin, R. C., Colina, L., & Finley, D. S. 1995, AJ, 110, 1316
Boggess, A., et al. 1978a, Nature, 275, 372
———. 1978b, Nature, 275, 377
Böhm-Vitense, E. 1980, ApJ, 239, L79
———. 1992, AJ, 109, 1539
———. 1993, AJ, 106, 1113
———. 1995, AJ, 110, 228
Burleigh, M. R., Jordan, S., & Schweizer, W. 1999, ApJ, 510, L37
Caplinger, J. 1995, *IUE* Newsletter, 54, 17
Dominy, J. F., & Lambert, D. L. 1983, ApJ, 270, 180
Dupuis, J., Fontaine, G., Pelletier, C., & Wesemael, F. 1992, ApJS, 82, 505
———. 1993a, ApJS, 84, 73
Dupuis, J., Fontaine, G., & Wesemael, F. 1993b, ApJS, 87, 345
Fekel, F. C., & Simon, T. 1985, AJ, 90, 812
Finley, D. S., Basri, G., & Bowyer, S. 1990, ApJ, 359, 483
Finley, D. S., Koester, D., & Basri, G. 1997, ApJ, 488, 375
Garhart, M. P., Smith, M. A., Levay, K. L., & Thompson, R. W. 1997, *IUE* Newslett., 57
Greenstein, J. L., & Oke, J. B. 1979, ApJ, 229, L141
Holberg, J. B., Ali, B., Carone, T. E., & Polidan, R. S. 1991, ApJ, 375, 716
Holberg, J. B., Barstow, M. A., & Sion, E. M. 1998, ApJS, 119, 207 (HBS)
Holberg, J. B., Forrester, W. T., & Shemansky, D. E. 1982, ApJ, 257, 656
Holberg, J. B., Wesemael, F., & Basile, J. 1986, ApJ, 306, 629
Koester, D., & Allard, N. 1993, in White Dwarfs, Advances in Observation and Theory, ed. M. A. Barstow (NATO ASI Series, V403), 237
Koester, D., & Holberg, J. B. 2001, in ASP Conf. Ser. 226, 12th European Conf. on White Dwarfs, ed. Provencal et al. (San Francisco: ASP), 299
Koester, D., Liebert, J., & Saffer, R. A. 1994, ApJ, 422, 783
Koester, D., Weidemann, V., Zeidler, K. T. E.-M., & Vauclair, G. 1985, A&A, 142, L5
Koester, D., Zukerman, B., Huensch, M., Wolff, B., & Reid, N. 2003, in 13th European Conf. on White Dwarfs, in press
Kondo, Y., et al. 1989, Exploring the Universe with the *IUE* Satellite (Dordrecht: Kluwer)
Landsman, W., Simon, T., & Bergeron, P. 1996, PASP, 108, 250
Liebert, J., Bergeron, P., & Holberg, J. B. 2002, AJ, 125, 348
Liebert, J., Wesemael, F., Hansen, C. J., Fontaine, G., Shipman, H. L., Sion, E. M., Winget, D. E., & Green, R. F. 1986, ApJ, 309, 241
Massa, D., & Fitzpatrick, E. L. 2000, ApJS, 126, 130 (MF00)
McCook, G. P., & Sion, E. M. 1999, ApJS, 121, 603 (MS99)
Nelan, E. P., & Wegner, G. 1985, ApJ, 289, L31
Nichols, J. S., & Linsky, J. L. 1996, AJ, 111, 517 (NL96)
Oswalt, T. D., Sion, E. M., Hammond, G., Vauclair, G., Liebert, J. W., Wegner, G., Koester, D., & Marcum, P. M. 1991, AJ, 101, 583
Provencal, J. L., Shipman, H. L., Thejll, P., Vennes, S., & Bradley, P. A. 1996, ApJ, 466, 1011
Schmidt, G., West, S. C., Liebert, J., Green, R. F., & Stockman, H. S. 1986, ApJ, 309, 218
Shipman, H. L. 1986, BAAS, 18, 952
Sion, E. M., Bruhweiler, F. C., Mullan, D., & Carpenter, K. 1989, ApJ, 341, L17
Sion, E. M., Greenstein, J. L., Landstreet, J. D., Liebert, J., Shipman, H. L., & Wegner, G. A. 1983, ApJ, 269, 253
Sion, E. M., Liebert, J., Vauclair, G., & Wegner, G. 1988, in White Dwarfs, ed. G. Wegner (Berlin: Springer), 354
Vennes, S., Christian, D. J., & Thorstensen, J. R. 1998, ApJ, 502, 763
Wegner, G. 1983, ApJ, 269, 253
Wegner, G., & Swanson, S. R. 1991, ApJS, 75, 507
Weidemann, V., & Koester, D. 1995, A&A, 297, 216
Wickramasinghe, D. T., & Ferrario, L. 2000, PASP, 112, 873
Wesemael, F., et al. 1994, ApJ, 429, 369
Wolff, B., Koester, D., & Liebert, J. 2002, A&A, 385, 995
Zeidler, K. T. E.-M., Weidemann, V., & Koester, D. 1986, A&A, 155, 356